REVIEW ARTICLE



Prussian Blue Analogues as Electrodes for Aqueous Monovalent Ion Batteries

Shen Qiu¹ · Yunkai Xu¹ · Xianyong Wu¹ · Xiulei Ji¹

Received: 26 July 2020 / Revised: 25 October 2020 / Accepted: 20 November 2020 © Shanghai University and Periodicals Agency of Shanghai University 2021

Abstract

Aqueous batteries have engendered increasing attention as promising solutions for stationary energy storage due to their potentially low cost and innate safety. In various aqueous battery systems, Prussian blue analogues (PBAs) represent a class of promising electrode materials with fascinating electrochemical performance, owing to their large open frameworks, abundant ion insertion sites, and facile preparation. To date, PBAs have shown substantial progress towards storage of alkali metal ions (Li⁺, Na⁺, and K⁺), H⁺, and NH₄⁺ in aqueous electrolytes, which, however, has yet not been specifically summarized. This review selects some representative research to introduce the progress of PBAs in these battery systems and aims to discuss the crucial role of ionic charge carrier in affecting the overall electrode performance. Besides, some critical knowledge gaps and challenges of PBA materials have been pointed out for future development.

Keywords Prussian blue analogues · Aqueous batteries · Monovalent ion storage ·

1 Introduction

The storage of renewable energy demands the development of advanced battery technologies that are sustainable, costeffective, and safe [1]. Currently, the prevalent lithium-ion batteries have dominated the market of mobile devices and electric vehicles due to their overwhelmingly high energy density (200–250 Wh kg⁻¹) [2]; however, the scarce reserve and the uneven distribution of Li will soon significantly restrict their further applications [3, 4]. Besides, the utilization of flammable and toxic aprotic solvents also incurs safety concerns. In this scenario, aqueous batteries that employ alternative ionic charge carriers represent an attractive solution for stationary energy storage [5–7]. Of note, the energy density is not a top priority for storage-type batteries. For example, lead-acid batteries afford a low energy density of only $\sim 30 \text{ Wh kg}^{-1}$ on the device scale [1], which, however, are still widely used in various applications. By contrast, the levelized energy cost, i.e., the cost per kWh

delivered, over cycling [8], cell safety, and environmental friendliness are critical considerations in electrical grids. Aqueous batteries that operate on Earth-abundant elements and mild electrolytes do not necessarily replace lithium-ion batteries but are promising to outperform lead-acid batteries, given a higher energy density and a longer cycling life [5–7].

Dahn et al. pioneered the aqueous Li-ion battery research in 1994, where the battery comprises the LiMn₂O₄ cathode, the VO₂ anode, and a 5.0 M (1 M=1 mol L⁻¹) LiNO₃ aqueous electrolyte [9]. This full cell chemistry operates on the prominent rocking-chair mechanism, which associates with the reversible shuttling of Li⁺ ions between cathode and anode structures. Notably, this cell design yields a cell voltage of 1.5 V without causing significant water electrolysis. Inspired by this study, researchers have practiced the similar wisdom to diversify aqueous batteries, where the choice of charge carriers extends to monovalent cations of Na⁺ [10], K⁺ [11], and NH₄⁺ [12], divalent Mg²⁺ [13], Ca²⁺ [14], and Zn²⁺ [15], and trivalent Al³⁺ [16]. Furthermore, the development of sophisticated electrolytes, such as concentrated or water-in-salt (WiS) electrolytes [17], has also brought the research of aqueous batteries to a new stage.

The development of competitive electrode materials is of the paramount importance for aqueous batteries, which entails the integration of excellent electrochemical performance, low cost, and the supply sustainability of materials

Published online: 03 March 2021



Department of Chemistry, Oregon State University, Corvallis, OR 97331-4003, USA

[18]. To date, metal oxides [19, 20], phosphates [21, 22], and polymers [23] have been widely investigated as electrodes in aqueous batteries, albeit with limitations observed. For instance, metal oxides are usually subjected to the compact lattice structures, which only allow the usage of Li⁺ and Na⁺ ions as charge carriers [24]. Phosphates possess robust polyanionic crystal structures, thus offering stable cycling; however, the mass burden of heavy [PO₄]³⁻ frameworks constrains the specific capacity to 60–120 mAh g⁻¹ [25]. Polymers are amenable to various ion storage due to their versatile functionality; however, the low tap density curbs their applications [26]. In comparison, Prussian blue analogues (PBAs) stand out as a group of attractive electrode materials in various battery systems due to their appealing large open structures, reversible redox chemistry, and versatile ion-storage capability [27-29]. Moreover, PBAs can be prepared from inexpensive raw materials by facile aqueous precipitation methods, which holds great promise in large-scale applications. Compared to metal oxides and phosphates that necessitate complicated solid-state reactions and a subsequent high-temperature annealing process [18–21], the preparation of PBAs at a mild temperature is more energy efficient, which lowers the cost.

PBAs are metal hexacyanoferrates with a nominal composition of $A_xM[Fe(CN)_6]\cdot mH_2O$, where A and M denote removable cations (Li⁺, Na⁺, K⁺, etc.) and transition metal ions (Fe, Co, Ni, and Cu, etc.), respectively [30, 31]. The number of zeolitic water (m) often depends on the ambient conditions such as moisture and temperature, whereas the content of extractable cations (x) depends on the valence states of transition metals [32]. The three primary stoichiometries of PBAs are $M^{III}[Fe^{III}(CN)_6]$, $AM^{III}[Fe^{II}(CN)_6]$ (or $AM^{II}[Fe^{III}(CN)_6]$), and $A_2M^{II}[Fe^{II}(CN)_6]$ are dubbed as Prussian yellow analogue (PYA), Prussian blue analogue (PBA), and Prussian white analogue (PWA), respectively

[33]. For simplicity, these materials can be abbreviated as MFe-PYA, MFe-PBA, and MFe-PWA, respectively. Figure 1a illustrates the crystal structure of an intact unit cell of M^{III}[Fe^{III}(CN)₆]·2H₂O. In this face-centred cubic (FCC) structure, Fe and M ions are octahedrally coordinated to carbon and nitrogen atoms of cyanide groups, respectively, and the alternating connection of the Fe-CN-M bonds further builds up a three-dimensional porous structure to host various guest ions [34, 35]. However, during the conventional rapid precipitation process of preparation, PBA compounds are prone to the formation of Fe(CN)₆ vacancies, which leads to a more general formula of $A_rM[Fe(CN)_6]_{1-\nu} \cdot \square_{\nu} \cdot mH_2O$ (☐ represents the vacancy) [29, 34]. For better visualization, Fig. 1b shows the crystal structure of a defective $M^{III}[Fe^{II}(CN)_6]_{3/4}\cdot \square_{1/4}\cdot 3.5H_2O$, which misses 1/4 of Fe(CN)₆ sites as vacancies that perfectly reside in each cubic centre [36]. Consequently, six ligand water molecules will be present in the vacancy sites, which are coordinated to nearby M ions. However, we need to note that in samples of PBAs, these vacancies distribute randomly throughout the entire crystal structures.

PBAs exhibit multifaceted advantages as appealing electrodes for aqueous batteries. Firstly, they can potentially undergo two-electron reactions based on Fe^{III}/Fe^{II} and M^{III}/M^{II} redox couples, which gives rise to high theoretical capacities of 155–190 mAh g⁻¹ for Li⁺, Na⁺, and K⁺ insertion [37]. Such capacity values surpass phosphate materials (60–120 mAh g⁻¹) and rival metal oxides and polymers. Secondly, the Fe^{III}/Fe^{II} and M^{III}/M^{II} redox couples usually provide high reaction potentials of 0.6–1.2 V vs. the standard hydrogen electrode (SHE) [38–40], which are beneficial to increase the full cell output voltage. Thirdly, the 3D framework with open <100> channels (3.2 Å in diameter) and interstitial nanocavities (4.6 Å in diameter) not only endows fast insertion kinetics but also facilitates the storage

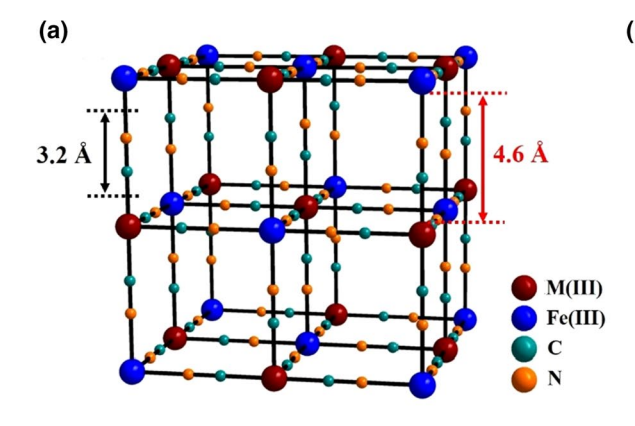
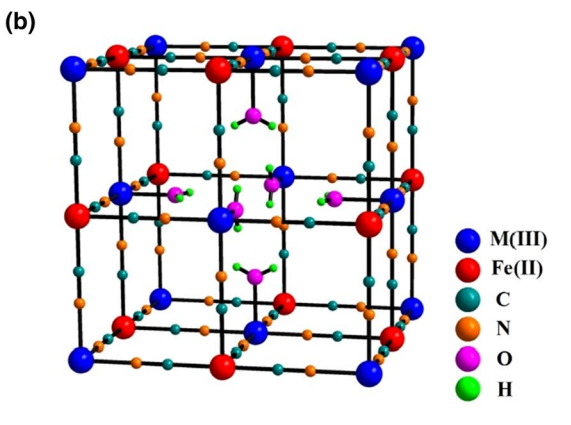


Fig. 1 a The crystal structure of an intact $M^{III}[Fe^{III}(CN)_6]\cdot 2H_2O$. **b** The crystal structure of a defective $M^{III}[Fe^{II}(CN)_6]_{3/4}\cdot \Box_{1/4}\cdot 3.5H_2O$. The zeolitic water molecules that reside in the sub-cube centre are not



shown for clarity. Reproduced with permission from Ref. [29]. Copyright 2016, American Chemical Society



of a wide spectrum of cations such as H^+ , Li^+ , Na^+ , K^+ , and NH_4^+ [41]. Table 1 shows the physicochemical properties of these monovalent ions [42, 43]. Fourthly, the open PBA structure minimizes the lattice expansion/shrinkage during the ion (de)insertion, which is conducive to the cycling stability [34]. For instance, the volume change of NH_4^+ insertion in FeFe-PBA is found lower than 1% [44], which pertains to a zero-strain insertion reaction and thus leads to superior cycling of 50000 cycles. Last but not least, PBA compounds are insoluble precipitates with extremely low solubility product constants ($k_{\rm sp}$), which effectively circumvents the troublesome material dissolution in water.

Due to these conspicuous advantages, PBAs have attracted increasing attention as universal electrodes for various ion storage, such as monovalent metal ions (H⁺, Li⁺, Na⁺, K⁺, NH₄⁺, Rb⁺, and Cs⁺) [45], alkaline earth metal ions (Mg²⁺, Ca²⁺, Sr²⁺, and Ba²⁺) [46], trivalent ions (Al³⁺) [47], and transition metal ions (Fe²⁺ and Zn²⁺) [48, 49]. Particularly, the redox chemistry of PBAs in aqueous monovalent metal ion batteries has been extensively studied [50, 51], which translates to promising electrode performance in terms of capacity, rate capability, and cycling stability. Furthermore, from the perspective of designing full cells, aqueous monovalent metal ion batteries seem to be closer to practical applications than divalent and trivalent ion batteries [6]. In this minireview, we highlight some of the most representative studies to provide a sketch picture of PBA materials in aqueous monovalent ion batteries, where the scope covers Li⁺, Na⁺, K⁺, H⁺, and NH₄⁺. We also compare and discuss the performance disparity of PBAs in storing different ions, which pinpoints the critical role of the ion-electrode interplays for electrochemical properties of rechargeable batteries.

2 PBA Electrodes for Monovalent ion Storage

In 1978, Neff et al. reported the first electrochemical synthesis of FeFe-PBA in an aqueous K-containing mixture solution of K_3 Fe(CN)₆ and FeCl₃ [52]. This electrode exhibits one pair of oxidization/reduction (ox/re) peaks at 0.46/0.44 V versus standard hydrogen electrode (SHE), which is attributed to the reversible K^+ insertion into the

Table 1 The physicochemical properties of various monovalent ions

	H ⁺	Li ⁺	Na ⁺	K ⁺	NH ₄ ⁺
Molar mass (g mol ⁻¹)	1.0	6.94	23.0	39.1	18.0
Naked ion radius (Å)	0.89×10^{-5}	0.76	1.02	1.38	1.48
Hydrated ion radius (Å)	1.0 ± 0.1	3.82	3.58	3.31	3.31
Ionic mobility	36.23	4.01	5.19	7.62	7.62

PBA lattice. Later, extensive efforts have focused on PBA thin-film electrodes in various applications of electrocatalysts, electroanalysis, and electrochromism, etc. [36, 53–56]. It has been well documented that the large open PBA structure exhibits a high preference towards bulky cations such as K⁺, NH₄⁺, Rb⁺, and Cs⁺, whereas smaller ions such as Li⁺ and Na⁺ block the redox reversibility [53–56]. For instance, Itaya et al. reported that FeFe-PBA supports highly reversible NH₄⁺ and Rb⁺ insertion for 1000 cycles in cyclic voltammetry (CV) tests, which greatly exceeds the short 2-10 cycles for Li⁺ and Na⁺ ions [54]. Scholz et al. revealed the effect of transition metal ions of the framework on the redox potentials of PBAs, where a higher charge/radius ratio of M^{n+} ions generally elevates the ion (de)insertion potentials [57]. These early studies on PBA thin-film electrodes in 1980-2000 have paved the way for the subsequent PBA applications in aqueous batteries. However, it was until 2011 when Cui et al. pioneered the study of bulk PBA electrodes in aqueous K⁺ batteries [11], which revived the interests of PBAs in various battery systems. Here, we will introduce the progress of PBA materials in the order of aqueous Li⁺, Na⁺, K⁺, NH₄⁺, and H⁺ ion batteries.

2.1 Aqueous Lithium-Ion Batteries

Among various aqueous batteries, aqueous Li-ion batteries have made the most significant progress in terms of electrode materials, electrolytes, and full cells [58, 59]. Nevertheless, PBAs have been rarely reported for Li⁺ storage in aqueous electrolytes, which likely results from the size mismatch between the PBA's ionic channels (3.2 Å) [41] and hydrated Li⁺ ions (3.82 Å) [42]. Due to the strong electrostatic interactions between Li⁺ ions of high charge density and the solvation sheath of water, the in-coming Li⁺ ions cannot be fully dehydrated upon the insertion into PBA frameworks, which causes severe structure degradation and even dissolution of the PBA electrode in aqueous Li⁺ electrolytes.

In 2011, Cui et al. pioneered the comparative study of two kinds of NiFe and CuFe-PBAs for the insertion of Li⁺, Na⁺, K⁺, and NH₄⁺ [45]. In these two materials, only the carbon-coordinated Fe^{III}/Fe^{II} (abbreviated as C- Fe^{III}/Fe^{II}) couples are redox-active, whereas the Ni and Cu ions are inert and can stabilize the structures. Interestingly, the ion insertion potential increases with the increment of cation radii (NH₄⁺ > K⁺ > Na⁺ > Li⁺), where Li⁺ insertion shows the lowest potential of 0.6 V vs. SHE, 0.4 V lower than that of NH₄⁺ insertion. In addition, Li⁺ insertion demonstrates multiple pairs of broad redox peaks, which contrasts with the well-resolved single pair of Na⁺, K⁺, and NH₄⁺ insertion. It is likely that partially hydrated Li⁺ ions may occupy different crystal sites in PBA structures such as the zeolitic and



Fe(CN)₆ vacancy sites, which results in the multiple redox CV peaks [45].

Another drawback of Li⁺ insertion in PBAs is the poor cycling performance. Figure 2a, b shows the CV curves of the FeFe(CN)₆ electrode for Na⁺ and Li⁺ storage, respectively [60]. Evidently, the Na⁺ storage is featured with high reversibility, whereas the Li⁺ insertion suffers fast capacity fading with the presence of complicating CV peaks. Besides, this electrode shows lower redox activity (smaller CV areas) at higher potentials, which suggests the suppression effect of Li⁺ ions on the C-Fe^{III}/Fe^{II} couple. To understand the structural evolution, Li et al. compared the XRD patterns of the pristine, discharged, and charged FeFe(CN)₆ materials [60]. Interestingly, Na⁺ insertion expands the lattice parameter from 10.18 to 10.64 Å (Fig. 2c), while there is no peak shift for Li⁺ insertion (Fig. 2d). The authors proposed that partially hydrated Li⁺ ions may either accumulate near the surface of small grains or reside in the large open sites such as Fe(CN)₆ vacancies [60]. They also discovered that after repeated Li⁺ insertion, the morphology of PBAs is transformed from the pristine nano-cubes to some petaloid-like structures, which indicates the structure degradation.

2.2 Aqueous Sodium-Ion Batteries

Compared to Li counterparts, aqueous Na-ion batteries hold more promise for large-scale energy storage, due to greater abundance and wider availability of Na sources on the Earth [21, 55]. More importantly, the comparatively larger Na⁺

ions can better fit into the PBAs' voids, which facilitate the PBA performance [61]. To date, a number of PBA compounds, particularly NiFe [62, 63], CuFe [64, 65], FeFe [66], CoFe [67], and MnFe [68], have been widely investigated for aqueous Na⁺ storage, which have demonstrated excellent electrode performance. Among them, NiFe and CuFe-PBAs usually experience the one-electron transfer reaction based on the Fe^{III}/Fe^{II} redox couple [62–65], whereas FeFe, MnFe, and CoFe-PBAs are amenable to the two-electron reaction via both Fe^{III}/Fe^{II} and M^{III}/M^{II} couples [66–68].

In 2011, Cui et al. first conducted the study of PBAs in aqueous Na-ion batteries [62]. They reported that a NiFe-PBA of $K_{0.5}Ni[Fe(CN)_6]_{0.83} \cdot 3.0H_2O$ delivers a reversible capacity of ~ 58 mAh g⁻¹ at 0.83 C, which still retains ~ 40 mAh g⁻¹ at a high rate of 41.7 C (Fig. 3a). Note that the mass loading of this electrode is between 7 and 12 mg cm⁻², which is higher than most other PBA reports. This electrode also offers excellent cycling stability with negligible capacity fading over 5000 cycles [62]. Ex situ XRD patterns reveal that NiFe-PBA maintains well its cubic structure without a phase transition, and the reversible Na⁺ insertion merely results in a trivial lattice change of 0.18% [62]. The S-shaped charge/discharge curves in Fig. 3a imply the solid solution reactions during (de)insertion of Na+ ions. However, this material occurs in its oxidized form with predominant Fe³⁺ ions, which necessitates chemical or electrochemical prereduction for the full cells unless the anode contains extractable Na⁺ ions. To address this issue, Yang et al. prepared a Na-rich NiFe-PWA of Na_{1.88}Ni[Fe(CN)₆]_{0.97}·4.7H₂O, which

Fig. 2 a CV curves of FeFe(CN)₆ for Na⁺ (de)insertion. b CV curves of FeFe(CN)₆ for Li⁺ (de)insertion. c Ex situ XRD patterns for Na⁺ insertion. d Ex situ XRD patterns after Li⁺ (de)insertion. Reproduced with permission from Ref. [60]. Copyright 2018, Elsevier

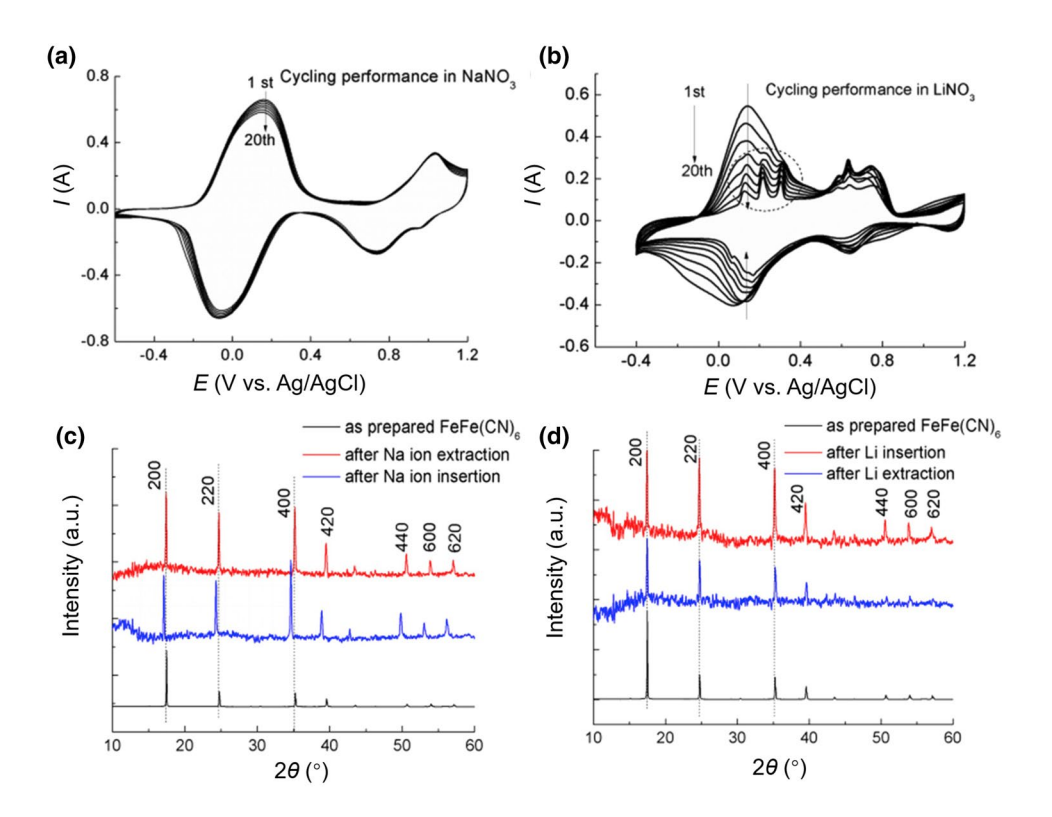
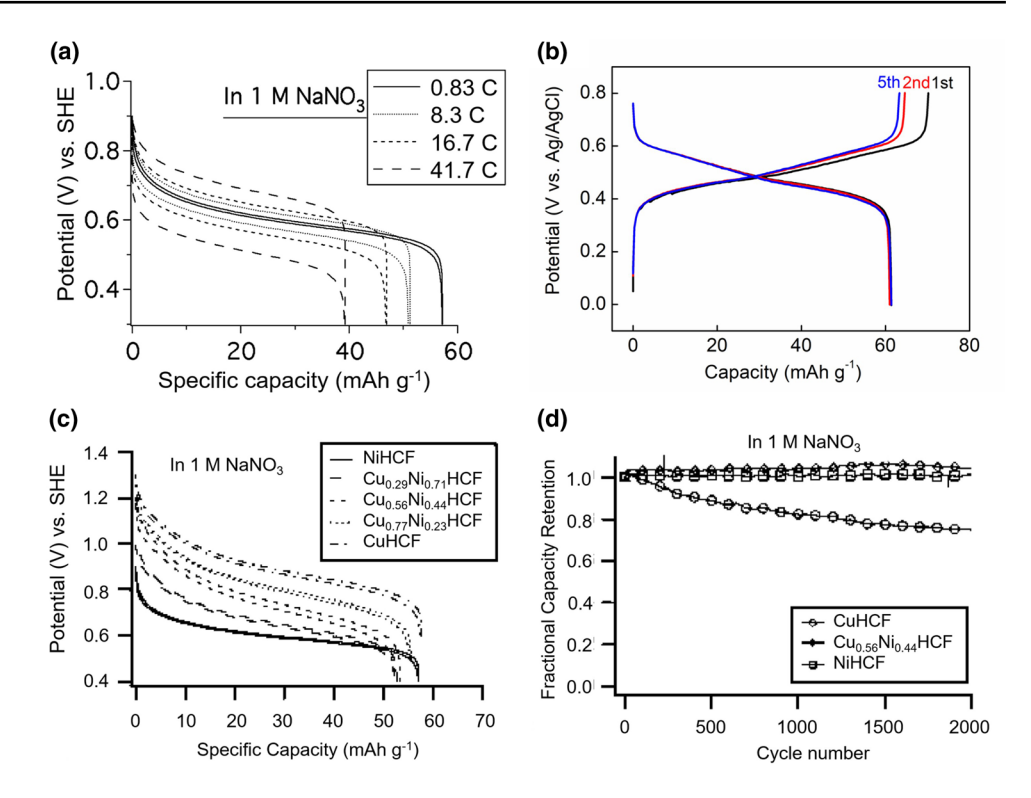




Fig. 3 a The rate performance of NiFe-PBAs in 1 M NaNO3 electrolytes (acidified to pH=2). Reproduced with permission from Ref. [62]. Copyright 2011, American Chemical Society. b The charge/ discharge curves of Na-rich NiFe-PWAs. Reproduced with permission from Ref. [63]. Copyright 2013, Elsevier. c The comparison of charge/discharge curves for Cu, Ni(1-x)Fe-PBAs. d The cycling comparison of Cu_xNi_(1-x)Fe-PBAs in 1 M $NaNO_3$ electrolytes (pH = 2). Reproduced with permission from Ref. [69]. Copyright 2011, American Chemical Society



affords the initial charge process (Fig. 3b) [63]. When paired with the $NaTi_2(PO_4)_3$ anode, the aqueous Na-ion full cell realizes a cell voltage of ~1.27 V and an energy density of 42.5 Wh kg⁻¹ based on the mass of two electrodes.

Another issue of NiFe-PBAs is their moderate operation potential of +0.5 V vs. Ag/AgCl, which limits the full cell voltage. To elevate the insertion potential, a feasible strategy is to dope Cu that shows a stronger inducing effect on the Fe^{III}/Fe^{II} couple [57, 64]. Cui et al. prepared a series of Cu_xNi_(1-x)Fe-PBAs with different stoichiometries, which retain the typical cubic crystal structure without phase separation [69]. Consequently, the reaction potentials of these PBAs readily vary with the Cu/Ni atomic ratios, where a greater Cu content leads to a higher potential (Fig. 3c). Additionally, due to the stabilization effect of Ni ions, Cu_rNi_(1-x)Fe-PBAs also achieves excellent cycling performance of ~ 100% capacity retention over 2000 cycles, which surpasses CuFe-PBAs (Fig. 3d) that suffers from 25% capacity loss. This doping strategy offers leeway to prepare PBA compounds with tunable crystal structures and better electrode performance [70, 71]. Later, Yang et al. prepared the Na-rich CuFe-PWA materials [65], which deliver a similar capacity of ~60 mAh g⁻¹ and a comparable reaction potential of +0.65 V vs. Ag/AgCl. It also exhibits a remarkable rate capability of 100 C and cycling stability of 1000 cycles in full cells, where the electrolyte is a near-neutral Na₂SO₄ solution.

Albeit the stable cycling of NiFe and CuFe-PBAs, their one-electron reaction mechanism has markedly restricted

the specific capacity to ~60 mAh g⁻¹. In pursuit of a higher capacity, it is imperative to investigate two-electron materials such as FeFe, CoFe, and MnFe-PBAs [66–68]. Particularly, FeFe-PBA stands out due to its prominence in the research history and the usage of inexpensive Fe elements. Unfortunately, early studies have suggested that Na⁺ ions would act as blocking ions that degrade the FeFe-PBA's redox chemistry [54, 55]. Indeed, there was no report of reversible two-Na⁺ reactions in the FeFe-PBA structure.

Recent studies have revealed that PBA structural properties have a large impact on its Na-insertion performance, and it is the structural vacancies that result in the poor Nainsertion reversibility [72, 73]. We need to note that conventional PBAs always contain a large number of Fe(CN)₆ vacancies (20%–30%) in their structures (Fig. 1b) due to the fast precipitation and crystallization process during preparation [74]. These structural vacancies render PBAs' structures brittle and fragile, which are susceptible to collapsing during the two-electron reactions associated with the lattice changes [30]. By contrast, one-electron-transfer electrodes, e.g., NiFe or CuFe-PBAs, are less sensitive to these vacancies, due to the inertness of nitrogen-coordinated M^{II} ions that can stabilize the structure. Thus, it is critical to understand the vacancy formation mechanism and eliminate these defects when necessary. From the perspective of coordination chemistry, it is thermodynamically favourable for M^{n+} ions to coordinate with N ligands of $[Fe(CN)]^{n-}$ groups in a 1:1 ratio, which is the driving force for the formation of a three-dimensional framework of -Fe-CN-M- bonds



[75, 76]. However, water molecules also act as competitive ligands to M^{n+} ions. During the rapid crystallization process, some $M^{n+}(H_2O)_m$ ions do not have sufficient time to be fully dehydrated. Thus, both M^{n+} and $M^{n+}(H_2O)_m$ participate in the coordination with $[Fe(CN)]^{n-}$ anions, which renders the presence of both Fe–CN–M and Fe–CN–M H_2O concurrently. These water molecules are strongly bound to transition metal ions (Fig. 1b), which is the root cause for the $Fe(CN)_6$ vacancy formation. In other words, the coordination between M^{n+} cations and $[Fe(CN)]^{n-}$ anions is thermodynamically favoured but kinetically challenged, which entails a slow crystallization process to fabricate low-vacancy PBAs [72–76].

Yang et al. have conducted intensive research to prepare low-defect PBAs for reversible two-Na⁺ storage [72, 73]. Figure 4a shows the slow precipitation process of Berlin green (BG), which is a green solid with a mixed state of Fe^{3+/2+}–CN–Fe³⁺ between PY (Fe³⁺–CN–Fe³⁺) and PB (Fe²⁺–CN–Fe³⁺) [72]. The initial mixing of Fe³⁺ and [Fe(CN)]³⁻ does not generate immediate precipitation but a dark brown solution, which corresponds to the formation of soluble Fe³⁺···[Fe(CN)₆]³⁻ complexes [77, 78]. Upon heating to 60 °C, the very oxidizing Fe³⁺···[Fe(CN)₆]³⁻ complexes gradually get reduced by chloride from the precursor or water

molecules [79], resulting in some Fe^{3+} ...[Fe(CN)₆]⁴⁻ species. It is known that the "insoluble" Prussian blue (IPB) of Fe[Fe(CN)₆]_{3/4} exhibits an extremely low solubility product constant, k_{sp} , which would serve as the nuclei for the subsequent crystal growth [80]. Due to the separated nucleation and growth processes, BG would grow into uniform nanocubes with significantly reduced vacancies (13% compared to 25% in IPB).

Yang et al. compared the charge/discharge performance of IPB and BG electrodes, respectively [72]. Due to the presence of Fe(CN)₆ vacancies and challenged structure integrity, the IPB electrode suffers from severe capacity fading with lower capacity utilization (Fig. 4c). On the contrary, the BG electrode demonstrates a highly reversible two-Na insertion reaction with an appreciable capacity of ~125 mAh g⁻¹ (Fig. 4d), which also retains 83% of its capacity after 500 cycles at a 10 C rate [67]. This study reveals the correlation between the PBA's structural defects and the two Na⁺ insertion performance, where a low-defect PBA structure is indispensable [72]. Later, Guo et al. reported a single iron-source method to prepare Na-rich FeFe-PWAs, which demonstrated an even higher capacity of ~ 150 mAh g⁻¹ for Na-storage [81]. Note that in the FeFe-PBA structure, the higher and lower reaction slopes stem from the

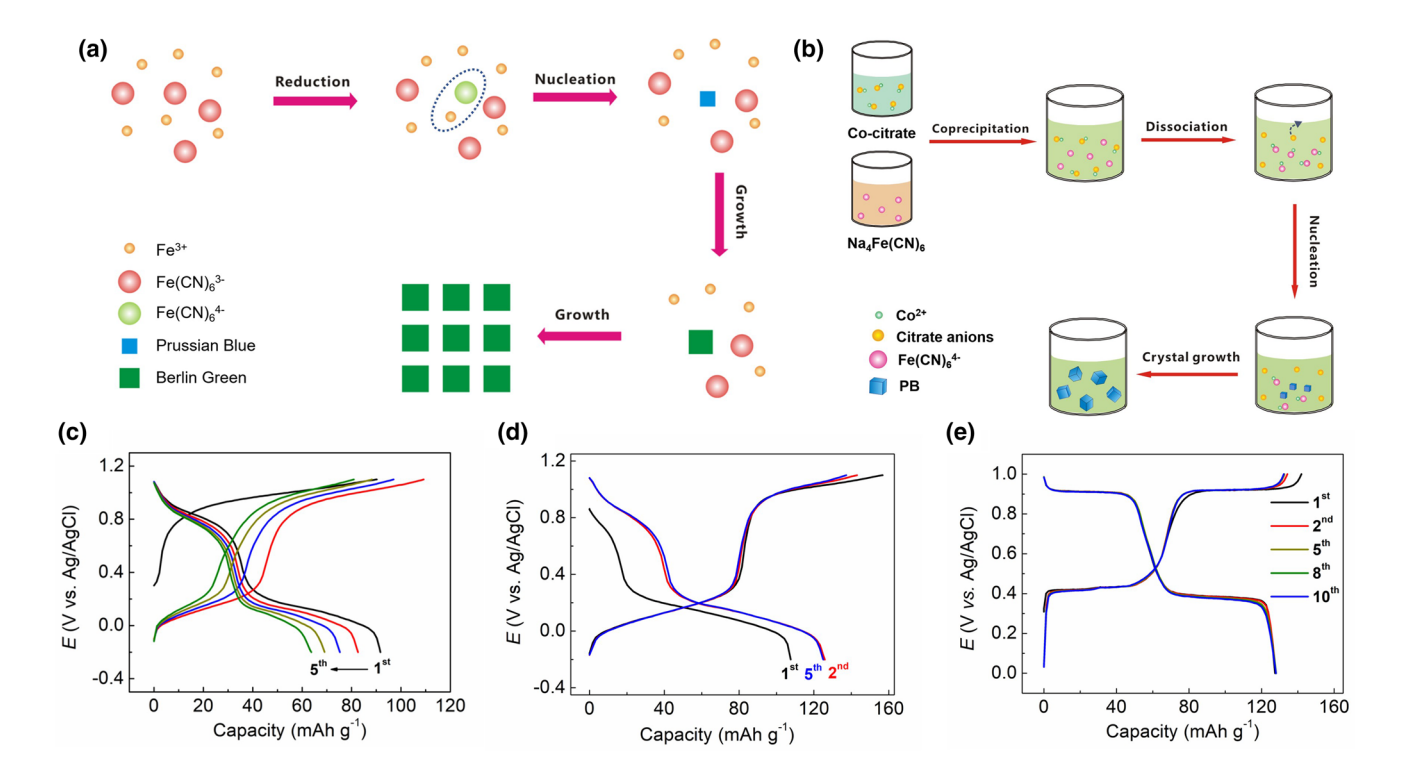


Fig. 4 a The synthetic mechanism of Berlin green nano-cubes. Reproduced with permission from Ref. [72]. Copyright 2015, Elsevier. **b** The controlled crystallization synthesis of Na-rich CoFe-PWA. Reproduced with permission from Ref. [67]. Copyright 2015, Wiley-VCH. **c** The charge/discharge profiles of conventional IPB electrodes.

Reproduced with permission from Ref. [72]. Copyright 2015, Elsevier. **d** The charge/discharge profiles of low-defect BG electrodes. Reproduced with permission from Ref. [72]. Copyright 2015, Elsevier. **e** The charge/discharge profiles of Na-rich CoFe-PWA. Reproduced with permission from Ref. [67]. Copyright 2015, Wiley-VCH



redox reactions of C-Fe^{III}/Fe^{II} and N-coordinated Fe^{III}/Fe^{II} (abbreviated as N-Fe^{III}/Fe^{II}) couples, respectively [72]. The A^+ insertion reaction is thus expressed as:

$$\begin{split} & \operatorname{Fe^{III}} \left[\operatorname{Fe^{III}}(\operatorname{CN})_{6}\right] + \operatorname{A^{+}} + \operatorname{e^{-}} \leftrightarrow \operatorname{AFe^{III}} \left[\operatorname{Fe^{II}}(\operatorname{CN})_{6}\right] \\ & \operatorname{AFe^{III}} \left[\operatorname{Fe^{II}}(\operatorname{CN})_{6}\right] + \operatorname{A^{+}} + \operatorname{e^{-}} \leftrightarrow \operatorname{A_{2}Fe^{II}} \left[\operatorname{Fe^{II}}(\operatorname{CN})_{6}\right] \end{split}$$

To further expand the applicability of low-defect PBAs, Hu et al. [82], Huang et al. [83], and Yang et al. [67] proposed to use complexing agents (such as citrate) to slow down the crystallization. As shown in Fig. 4b, citrate anion is a strong Lewis base towards Co²⁺ ions, where the equilibrium constant ($\log K_1$) is as high as 12.5 for Co²⁺·citrate³⁻ [67]. Such coordination effectively decreases the concentration of free Co²⁺ ions in the solution and thus slows down the initial nucleation process. The dissociation of citrate ions may also retard the crystal growth rate due to the possible steric hindrance effect. Consequently, the as-obtained CoFe-PWAs exhibit a desirable formula of $Na_{1.85}Co[Fe(CN)_6]_{0.99} \cdot \square_{0.01} \cdot 2.5H_2O$, which contains a minimal vacancy content of 1% and exhibits much larger crystal size of 300-600 nm [67]. Therefore, it realizes a highly reversible two-Na insertion reaction, with a high capacity of ~130 mAh g⁻¹ and two conspicuous plateaus at 1.1 and 0.6 V vs. SHE (Fig. 4e). The higher and lower reaction plateaus are attributed to the redox of C-Fe^{III}/Fe^{II} and N-Co^{III}/ Co^{II} couples, respectively [67]. When cycled at 5 C, it demonstrates 90% capacity retention over 800 cycles [67]. In comparison, the CoFe-PWAs synthesized without citrate exhibit lower capacity values and shorter cycling longevity. Due to the high capacity and high potential, the lowdefect CoFe-PWA was paired with the mainstream anode of $NaTi_2(PO_4)_3$, which gives rise to an energy density of ~67 Wh kg⁻¹ based on the active mass of both electrodes [67]. To further improve the cycling stability, Li et al. recently added a small amount of Co²⁺ ions (1% CoSO₄) into the 1 M Na₂SO₄ electrolyte, which further stabilizes the CoFe-PWA structure and suppresses the material dissolution [84]. Consequently, the electrode shows a prolonged cycling of 2000 cycles at a 10 C rate. However, we note that the presence of Co²⁺ ions will limit the cut-off potentials on the anode side, due to the high Co^{2+}/Co^{0} redox potentials (-0.28 V vs. SHE) [84]. This will prelude the use of low-potential anode materials such as NaTi₂(PO₄)₃, whose Na-insertion reaction takes place at -0.6 V vs. SHE [67].

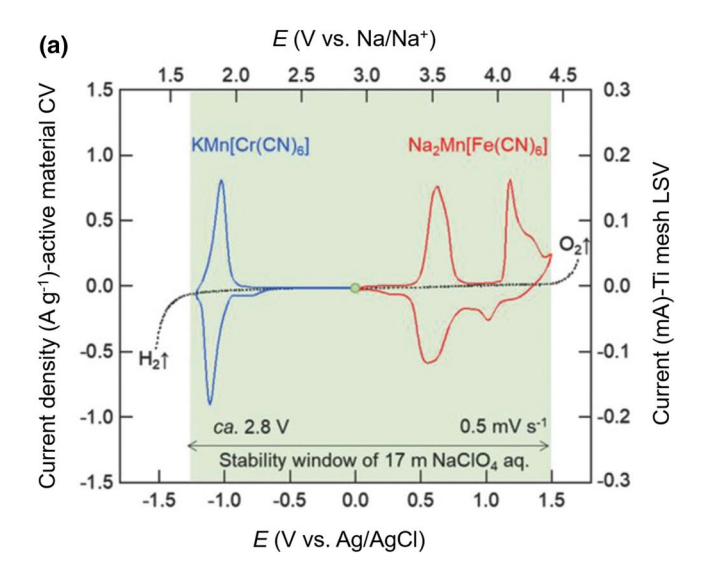
Due to the effectiveness of reducing structural defects, the controlled crystallization method has been widely utilized to synthesize other PBA materials with significantly improved performance [85–87]. An interesting work from Han et al. demonstrates that by using $[P_2O_7]^{4-}$ as the chelating agent, a highly crystalline CuFe-PBA with few vacancies was attainable [88]. As a result, this electrode would accommodate 1.5 Na⁺ insertion based on the C-Fe^{III}/Fe^{II} and N-Cu^{II}/Cu^I

couples, which leads to a high capacity of ~ 120 mAh g⁻¹ in non-aqueous electrolytes [88]. By contrast, the control sample is subject to 1 Na⁺ insertion with a compromised capacity of ~ 80 mAh g⁻¹. It would be interesting to examine its Na-insertion performance in aqueous electrolytes, which may rival the capacity of widely studied FeFe-PBAs and CoFe-PBAs [67, 72].

Regardless of the high capacity and high voltage of CoFe-PBAs, the expensive cobalt element will considerably increase the material cost. In comparison, MnFe-PBAs hold a great promise for aqueous Na-ion batteries, due to their high reaction potentials, rich elemental Fe/Mn abundance, and potentially low cost [88]. However, they are prone to material dissolution in aqueous electrolytes, which may arise from the relatively weak coordination of Mn²⁺ ions to N ligands [89]. Besides, the Jahn–Teller distortion effect of Mn³⁺ ions also imposes instability issues on the entire PBA framework [90]. Thus, even the low-defect MnFe-PWA cannot support a reversible two-Na reaction in conventional diluted aqueous electrolytes.

To tackle this challenge, Okada et al. first employed 17 m (1 m = mol kg⁻¹) NaClO₄ WiS electrolyte to inhibit the material dissolution [68, 91]. As shown in Fig. 5a, the MnFe-PWA electrode exhibits two pairs of ox/re peaks at 0.8 and 1.2 V vs. SHE, which is attributed to the redox couples of Fe^{III}/Fe^{II} and Mn^{III}/Mn^{II}, respectively. Such potentials exceed those of FeFe and CoFe-PBA materials [67, 72], which is advantageous to provide a higher energy density in full cells. Besides, it also offers a high specific capacity of ~ 110 mAh g⁻¹ (Fig. 5b), which is on par with FeFe and CoFe-PBAs [62, 67]. However, even in such concentrated electrolytes, this material still encounters appreciable capacity fading, where it loses 26% capacity over 100 cycles at 0.86 C. The potential explosion of the perchlorate salt under heat or collision also questions the applicability of such salts. Recently, Passerini et al. proposed to use the acetate-based WiS electrolytes to suppress the material dissolution [92]. However, acetate anions will be oxidized at higher potentials, which limits the MnFe-PWA electrode to the one-electron reaction (~75 $mAh g^{-1}$). Besides, the alkaline conditions of acetates may precipitate the transition metal ions in PBA frameworks, which restricts the cycling to 100 cycles. Most recently, Hu et al. demonstrated an ultra-high concentration electrolyte of 9 m sodium triflate (NaOTF) mixed with 22 m tetraethylammonium triflate (TEAOTF), which could efficaciously inhibit the MnFe-PWA material dissolution [93]. This cathode delivers a high capacity of 140 mAh g⁻¹ and stable cycling of 800 cycles in full cells at a 1 C rate. They coupled this cathode with the NaTiOPO₄ anode into a full cell, which delivers an average voltage of 1.74 V and a high energy density of 71 Wh kg⁻¹ based on the active mass of two electrodes. The practical energy





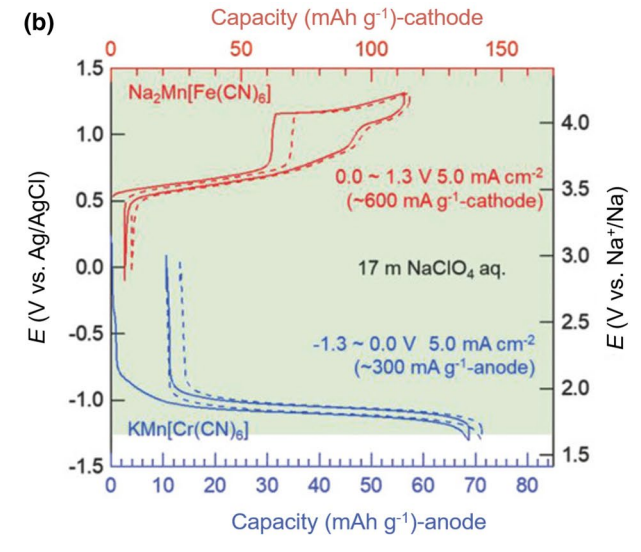


Fig. 5 a The CV curves of the $Na_2MnFe(CN)_6$ cathode and the $KMnCr(CN)_6$ anode in a 17 m (1 m=mol kg⁻¹) $NaClO_4$ WiS electrolyte. **b** The charge/discharge profiles of the $Na_2MnFe(CN)_6$ cathode

and the KMnCr(CN)₆ anode. Reproduced with permission from Ref. [91]. Copyright 2018, Wiley–VCH

density would approach $\sim 36 \text{ Wh kg}^{-1}$ on the device level, if we assume a mass burden of 50 wt% for inactive cell components such as conducting carbon, binders, electrolytes, and current collectors [94]. This value is better than lead-acid batteries (30 Wh kg⁻¹). However, we also note that the imperative use of large quantities of fluorinated salts will compromise the cell cost.

In addition to the aforementioned PBAs, ZnFe and VFe-PBAs have also received certain interests as Nastorage cathode materials [95-97]. However, they generally suffer from fast capacity fading in conventional electrolytes, which highlight the use of concentrated or highly acidic electrolytes. Qian et al. found that ZnFe-PWA shows severe material dissolution in 1 m NaClO₄ electrolytes, which translates to low capacity retention of 30% over 50 cycles [96]. When switched to 17 m NaClO₄ WiS electrolytes, the ZnFe-PWA demonstrates significantly improved cycling stability with negligible capacity fading [89]. Notably, this cathode shows a moderate capacity of 60 mAh g⁻¹ but a very high potential of 1.1 V vs. SHE, due to the inducing effect of Zn²⁺ ions on the Fe^{III}/Fe^{II} couple. Chung et al. investigated the VFe-PBA of Na_{0.133}(VO)[Fe(CN)₆]_{2/3}·4H₂O in a mixed electrolyte of 0.5 M Na₂SO₄ and 5.0 M H₂SO₄ [98]. By utilizing the VIII/VII and FeIII/FeII redox, this material delivers a reasonable capacity of 91 mAh g⁻¹. Notably, due to their high charge density, VIII ions are readily coordinated to water molecules or oxygen atoms, which explains the form of VO in the formula. This also accounts for their propensity to material dissolution, which leads to limited cycling of 250 cycles at 1.2 C.

2.3 Aqueous Potassium-Ion Batteries

The K^+ ion has a large ionic radius of 1.38 Å, which exceeds those of Li⁺ (0.76 Å) and Na⁺ (1.02 Å) [64]. This has markedly restricted the electrode choices for aqueous K-ion batteries, where a structure with large openings is a prerequisite. To date, among a handful of K-storage electrodes [99, 100], PBAs represent the most promising cathode materials due to their excellent structural compatibility towards K^+ ions. Accordingly, K^+ insertion not only exhibits a high potential but also renders excellent cycling stability [45].

In 2011, Cui et al. first investigated the K⁺ insertion in NiFe and CuFe-PBAs, which impressively deliver 5000 and 40000 cycles, respectively [62, 64]. The K⁺-storage reaction potential is 0.1–0.2 V higher than that of Na insertion, which benefits the full cell voltage. However, Fe ions in these structures exist in the +3 valance state, which cannot directly pair with K-deficient anodes in full cells. To address this issue, Zhao et al. prepared the K-rich NiFe-PWA of K₂NiFe(CN)₆·1.2H₂O [101], which delivers a capacity of $\sim 75 \text{ mAh g}^{-1}$ at 5 C and 40 mAh g $^{-1}$ at 500 C (Fig. 6a). When cycled at 30 C, it exhibits 98.6% capacity retention after 5000 cycles. Ex situ XRD patterns demonstrate that the lattice parameter slightly shrinks from 10.33 to 10.08 Å during K insertion [101], which accounts for the outstanding cycling. Interestingly, this electrode shows a plateau at 0.85 V vs. SHE (~0.6 V vs. SCE), which implies a two-phase



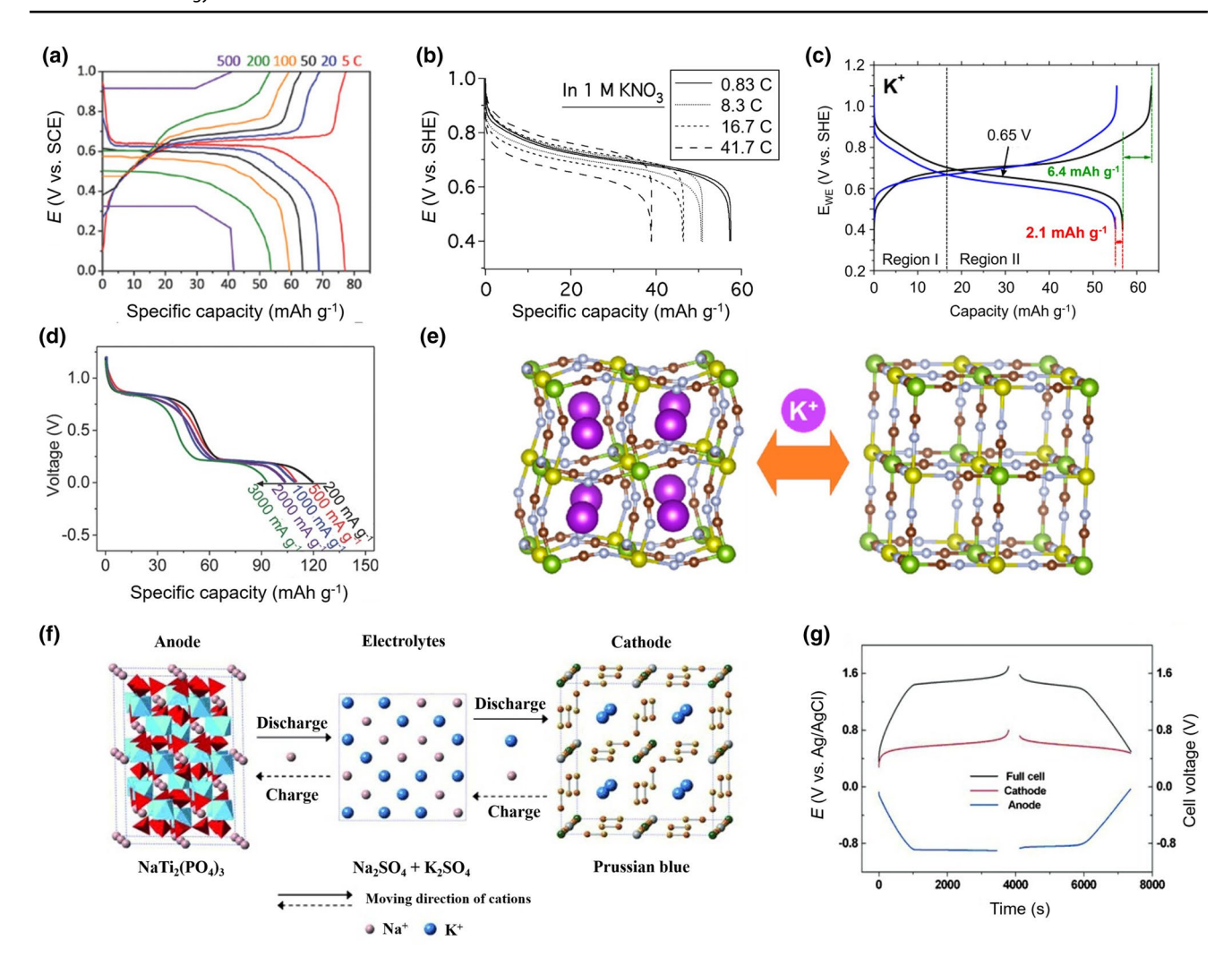


Fig. 6 a The charge/discharge profiles of K₂NiFe(CN)₆ electrodes. Reproduced with permission from Ref. [101]. Copyright 2018, Wiley–VCH. **b** The rate performance of KNiFe(CN)₆ electrodes. Reproduced with permission from Ref. [62]. Copyright 2011, American Chemical Society. **c** The charge/discharge profiles of K₂CuFe(CN)₆. Reproduced with permission from Ref. [103]. Copyright 2019, Elsevier. **d** The rate performance of K₂FeFe(CN)₆ electrodes. Reproduced with permission from Ref. [104]. Copyright

2016, Wiley–VCH. **e** The phase transition between monoclinic K_2 FeFe(CN) $_6$ and cubic FeFe(CN) $_6$. Reproduced with permission from Ref. [105]. Copyright 2017, American Chemical Society. **f** The working mechanism of an aqueous hybrid Na⁺/K⁺ ion battery. **g** The charge/discharge profiles of the cathode, the anode, and the full cell. Reproduced with permission from Ref. [97]. Copyright 2014, Wiley–VCH

reaction. However, the K-deficient NiFe-PBA in Cui et al.'s report demonstrates a smooth S-shaped slope (Fig. 6b), which corresponds to a solid-solution insertion process [62]. We deem that the high K content in $K_2NiFe(CN)_6$ may induce the phase transition from cubic to a monoclinic structure [102], which results in the two-phase reaction with flat plateaus. Recently, Anouti et al. also reported the performance of $K_2CuFe(CN)_6$ for K^+ storage [103], which shows a moderate capacity of ~55 mAh g⁻¹ (Fig. 6c) and stable cycling of 50 cycles (97% capacity retention).

Similarly, the one-electron reaction of NiFe and CuFe-PBAs limits the K-storage capacity, which highlights the need of two-electron-transfer PBAs. In this regard, Wang

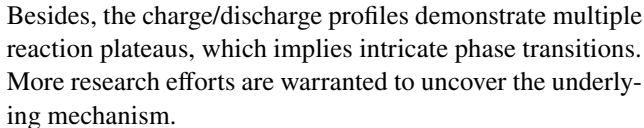
et al. synthesized well-defined $K_2\text{FeFe}(\text{CN})_6\cdot 2H_2\text{O}$ nanocubes by a single iron source method, where $K_4\text{Fe}(\text{CN})_6$ was used as a precursor in the presence of hydrochloric acid (HCl) [104]. Under the solvothermal conditions, a portion of $[\text{Fe}(\text{CN})_6]^{4-}$ anions will react with acids to form Fe^{2+} and HCN. The resultant Fe^{2+} ions further coordinate with the residual $[\text{Fe}(\text{CN})_6]^{4-}$ anions to grow into $K_2\text{FeFe}(\text{CN})_6\cdot 2H_2\text{O}$ crystals. This reaction has been reported in the Na-ion battery research by Guo et al., where the crystal growth is facilitated by the suppression of $\text{Fe}(\text{CN})_6$ vacancies [81]. However, this method generates highly toxic HCN, which can be replaced by the aforementioned citrate-assisted controlled crystallization method [67]. The



stoichiometric formula of this compound also needs to be accurately verified. This $K_2\text{FeFe}(\text{CN})_6$ electrode shows a high capacity of ~ 120 mAh g⁻¹ with two distinguishable plateaus at 1.0 and 0.5 V vs. SHE (Fig. 6d). In addition, it also exhibits excellent cycling of 500 cycles with nearly no capacity fading at both low (500 mA g⁻¹) and high current rates (3000 mA g⁻¹). Notably, compared to the S-shaped Na⁺ insertion in FeFe-PBA frameworks (Fig. 4d), the storage of bulky K⁺ ions exerts larger structural stress and thus distorts the cubic FeFe(CN)₆ structure into a monoclinic $K_2\text{FeFe}(\text{CN})_6$ one (Fig. 6e) [105], which results in the phase transition and reaction plateaus.

MnFe-PWA also operates on a two-electron reaction that corresponds to a high capacity. However, as discussed in the Na-ion section, MnFe-PWAs are vulnerable to the active material dissolution, which restricts their applications. To tackle this challenge, Hu et al. integrated the utilization of the 22 m potassium trifluoromethanesulfonate (KCF₃SO₃) WiS electrolyte and the Fe elemental doping, which mitigates the dissolution and stabilizes the structure synergistically [106]. Impressively, the MnFe-PWA exhibits a high capacity of ~ 130 mAh g⁻¹ without Fe/Mn dissolution, which significantly surpasses the performance in the dilute 1 m KCF₃SO₃ electrolyte. They further revealed that the undoped MnFe-PWA experiences a complicated phase transition of monoclinic PWA ↔ cubic PBA ↔ tetragonal PYA, whereas the Fe-doped one is subject to monoclinic PWA ↔ monoclinic/cubic PBA ↔ cubic PYA [106]. The introduction of Fe ions decreases the concentration of Mn³⁺ ions in the structure, which minimizes the Jahn-Teller distortion effect and circumvents the cubic/tetragonal transition. Consequently, the doped MnFe-PWA shows a superior lifespan of 10000 cycles at a 100 C rate. This electrode can also work in a wide temperature range from -20 to 60 °C [106]. The authors further paired the MnFe-PWA cathode with an organic anode of 3,4,9,10-perylenetetracarboxylic diimide (PTCDI), which gives rise to an aqueous K-ion full cell with an average voltage of 1.27 V and an energy density of 80 Wh kg⁻¹ based on the active mass of two electrodes [106]. Such energy density would be the highest among reported aqueous K-ion batteries, which may still reach 40 Wh kg⁻¹ if we assume a 50 wt% dead mass burden [94]. However, the use of expensive and hazardous fluorinated salts may bring about cost and safety concerns.

To our knowledge, the K-insertion in CoFe-PWA has not been reported in aqueous electrolytes. Our recent work reveals that this compound shows a low capacity of ~ 60 mAh g⁻¹ in non-aqueous electrolytes [100], which corresponds to a one-electron reaction. Previous studies suggest that the Co^{III}/Co^{II} redox couple is sensitive to local environments in PBAs [107–109], where the absence of Fe(CN)₆ vacancies and the employment of small cations such as Na⁺ are indispensable for two-electron reactions [101, 102].



Albeit the attractive K-insertion performance in PBA structures, the bulky K⁺ size has dramatically limited the development of suitable K-storage anode materials. As a compromise, PBAs have also been used as feasible cathodes in hybrid ion battery systems [110]. Figure 6f illustrates the working mechanism of a hybrid Na⁺/K⁺ ion battery, where the cathode, the anode, and the electrolyte are $K_{0.08}Ni_{0.75}Zn_{0.70}[Fe(CN)_6]$, $NaTi_2(PO_4)_3$, and a mixed solution of 0.4 M K₂SO₄ + 0.1 M Na₂SO₄, respectively [97]. Upon charge/discharge, the cathode will preferentially accommodate K⁺ over Na⁺ ions due to the higher K-insertion potential by 0.1-0.2 V, whereas the anode will exclusively host Na⁺ ions due to the moderate interstitial sites in the phosphate frameworks [97]. The ionic selectivity is central to such a hybrid ion battery configuration, which effectively addresses the issue of lacking K-storage anode materials. Additionally, compared to the sole Na⁺ insertion, the hybrid ion design enjoys an extra voltage increase due to the higher K⁺ insertion potentials. For example, the full cell thus delivers an improved voltage of ~1.45 V and 53 Wh kg⁻¹ based on the active mass of two electrodes (Fig. 6g). This hybrid ion battery concept is also applicable to other battery systems, such as Li⁺/Na⁺ [111], Li⁺/K⁺ [97], Na⁺/ NH_4^+ [44], and Li⁺/Fe²⁺ [49]. However, we need to point it out that the electrolyte is also a part of active materials for hybrid battery systems, which needs to be taken into account when calculating the device energy density. This issue resembles the case of dual-ion batteries to some extent, where a concentrated electrolyte would alleviate the electrolyte mass burden [112].

2.4 Aqueous Ammonium-Ion Batteries

Compared to metal ions of Li⁺, Na⁺, and K⁺, non-metal ions of NH_4^+ have received less attention as alternative charge carriers, possibly due to the very large ionic radius of 1.48 Å [45]. However, such an ion size would perfectly match with the interstitial sites in PBAs, which results in high reaction potential and stable cycling. Moreover, NH_4^+ ions dissociate a small amount of protons in water, which provides a relatively acidic condition to further benefit the PBA cycling. Note that in previous studies, researchers have added extra acids (pH=2) to stabilize the PBA cycling for Na⁺ and K⁺ insertion [62, 64].

Cui et al. pioneered the $\mathrm{NH_4}^+$ insertion in NiFe and CuFe-PBAs, which exhibit high potentials and stable cycling of 500 cycles [45]. However, these two PBAs have no removable $\mathrm{NH_4}^+$ ions in the pristine structure, which challenges the



full cell implementation. Besides, the potentially appealing NH₄⁺ insertion chemistry warrants further investigation. Of note, Li⁺, Na⁺, and K⁺ are monoatomic ions with a spherical configuration, whereas NH₄⁺ is a polyatomic ion with a tetrahedral configuration, which may result in distinctive topochemistry or an ion diffusion mechanism [12].

To further test NH₄⁺ as a charge carrier for energy storage, our group presented a rocking-chair NH₄⁺-ion full cell, which works on the NH₄⁺ shuttling between the NiFe-PWA cathode and an organic anode of 3,4,9,10-perylenetetracarboxylic diimide (PTCDI) [113]. This NH₄+-rich PWA was prepared by an aqueous ion-exchange method, where its Nacontaining PWA version is mixed in a (NH₄)₂SO₄ solution under stirring for several hours. Due to the higher structure affinity to large ions, all the Na⁺ ions in the lattice are readily replaced by NH₄⁺ ions. More interestingly, it was found that the NiFe-PWA framework crystallizes in a cubic structure when NH₄⁺ ions are present, whereas it adopts a distorted monoclinic one when hosting Na⁺ ions (Fig. 7a) [113]. The disparity of phases implies the better structural compatibility of PBAs with $\mathrm{NH_4}^+$ ions. Ex situ XRD patterns also uncover that the NiFe-PWA maintains a cubic structure without any phase transition for NH₄⁺ (de)insertion. This electrode shows a specific capacity of ~60 mAh g⁻¹ (Fig. 7b) and stable cycling of 2000 cycles. Besides, it offers a higher potential by ~0.2 V than Na⁺ insertion, which benefits the full cell voltage. The ammonium full cell based on the NiFe-PWA cathode and the PTCDI anode offers a reasonable energy density of 43 Wh kg⁻¹ (based on the active mass of two electrodes) and stable cycling of 1000 cycles.

Later, Wu et al. investigated the $\mathrm{NH_4}^+$ insertion in the CuFe-PBA, which shows a similar capacity of ~60 mAh g⁻¹ and good cycling of 1000 cycles [114]. When paired with the Zn metal anode, this hybrid full cell affords a high voltage of ~1.8 V, which results from the 0.2 V higher $\mathrm{NH_4}^+$ insertion potential than $\mathrm{Zn^{2+}}$ ions. The hybrid cell thus delivers a high energy density of 114 Wh kg⁻¹ based on the two electrodes' active mass. However, the electrolyte also needs to be considered as an active mass in hybrid cells, which will dramatically decrease the practical energy density due to the diluted concentration [114].

It is appealing to explore whether $\mathrm{NH_4}^+$ ions would exert a two-electron reaction in PBA frameworks. In this respect, our group investigated $\mathrm{NH_4}^+$ insertion in BG with a comparison to Na^+ and K^+ ions [44]. As shown in Fig. 7c, BG exhibits only one pair of CV peaks for $\mathrm{NH_4}^+$, which contrasts with the well-defined two pairs of Na^+ and K^+ insertion. Even scanned to a very high potential of 1.7 V vs. SHE, the redox activity of the C-Fe^{III}/Fe^{II} couple is still not triggered. This one-electron reaction limits the capacity to ~90 mAh g⁻¹. However, due to the remarkable match of $\mathrm{NH_4}^+$ with the open PBA cavities, the BG electrode experiences

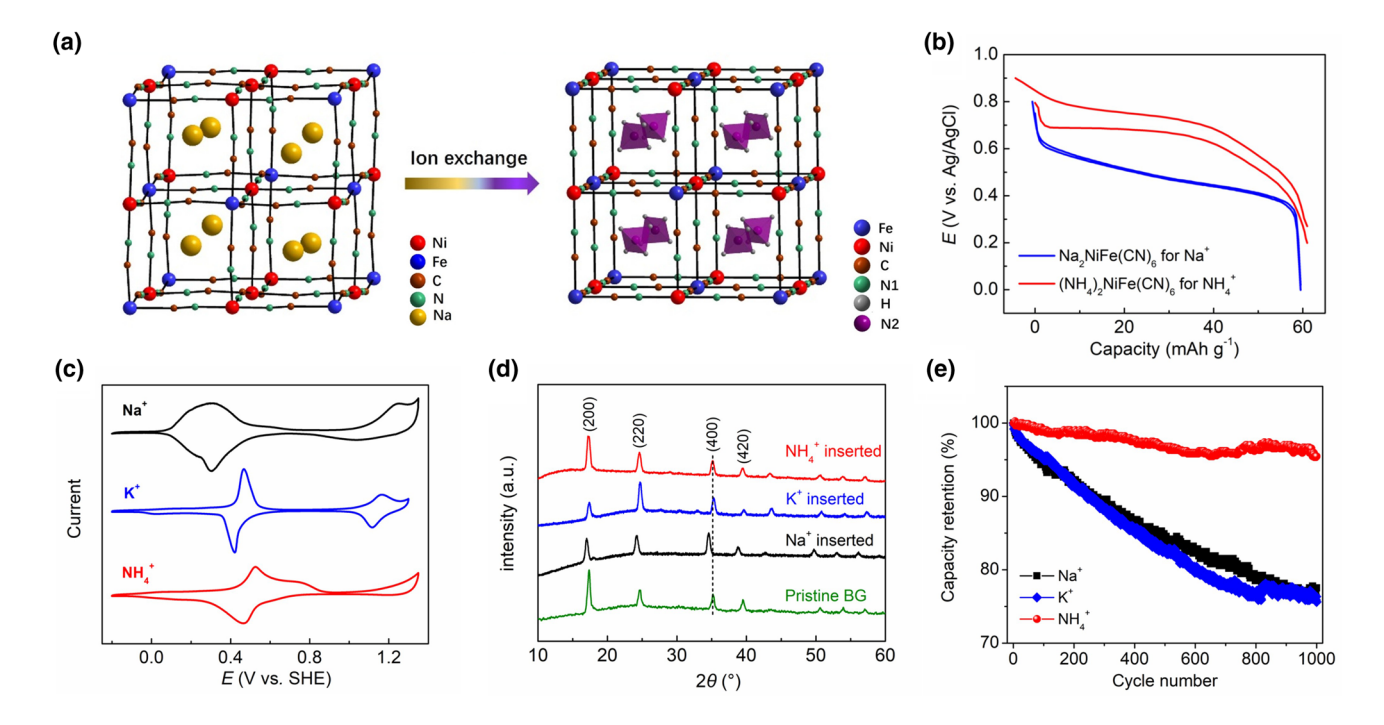


Fig. 7 a The scheme of the ion-exchange method to prepare $\mathrm{NH_4}^+$ -rich PWAs. **b** The charge/discharge profiles of the $\mathrm{Na_2NiFe}(\mathrm{CN})_6$ and $(\mathrm{NH_4})_2\mathrm{NiFe}(\mathrm{CN})_6$ electrodes. Reproduced with permission from Ref. [113]. Copyright 2017, Wiley–VCH. **c** The CV curves comparison of the FeFe(CN) $_6$ for Na $^+$, K $^+$, and NH $_4^+$ inser-

tion. **d** The ex situ XRD patterns for Na^+ , K^+ , and NH_4^+ insertion. **e** The cycling comparison for Na^+ , K^+ , and NH_4^+ insertion. Reproduced with permission from Ref. [44]. Copyright 2018, American Chemical Society



a zero-strain $\mathrm{NH_4}^+$ insertion process with negligible lattice change (Fig. 7d), which results in the exceptionally stable cycling of 50000 cycles with 78% retention [44]. By contrast, Na^+ insertion would significantly expand the BG lattice due to the $\mathrm{H_2O}$ co-insertion, whereas K^+ insertion will induce a phase transition from cubic to a monoclinic one (Fig. 7d) [44]. Consequently, BG shows much poorer cycling for Na^+ and K^+ insertion (Fig. 7e).

To date, CoFe and MnFe-PBAs have yet to be reported in NH_4^+ ion batteries. It would be interesting to learn if they can operate on two-electron NH_4^+ -insertion reactions.

2.5 Aqueous Proton-Ion Batteries

A proton represents an intriguing charge carrier due to its salient advantages of being minimal in size (\sim 0.89 femtometer) and light in mass (+1.0 g mol⁻¹) [115, 116]. These features may facilitate high specific capacities and fast kinetic properties. Moreover, it has been widely reported that the addition of some acids (protons) can lead to better cycling for PBAs [62, 64]. However, from the perspective of PBA insertion chemistry, protons would not be the first choice, considering the trend of ion preference in the order of NH₄ $^+$ > K $^+$ > Na $^+$ > Li $^+$ [55]. Besides, previous studies had suggested the small proton as a blocking ion for PBA

thin-film electrodes [117]. Indeed, even the low-defect BG cannot support reversible H⁺ insertion. As shown in Fig. 8a, the BG electrode not only suffers from appreciable capacity fading within several cycles, but also exhibits tapered redox current for the C-Fe^{III}/Fe^{II} couple. These challenges may account for the few studies of PBAs for proton insertion.

However, proton insertion in PBAs still shows advantages in aspects of reaction potentials and rate performance. Cui et al. reported that NiFe-PBA shows a pair of ox/re peaks at 0.6 V vs. SHE in acidic solutions (pH=3, Fig. 8b), which exceeds the Li^+ storage potential (1.0 M, pH = 2) and approaches that of Na⁺ ions [118]. If tested in the same concentration (1.0 M), the proton-storage potential would be further increased by $0.059 \times 3 = 0.177$ (V) according to the Nernst equation [119]. It is likely that hydrated protons such as hydronium (H₃O⁺) [120] serve as viable charge carriers to match the PBA nanocavities. Alternatively, naked protons can bind with lattice water to form interstitial hydroniums. Note that hydronium (H₃O⁺) shows a moderate ionic radius of $(1.0 \pm 0.1) \text{ Å}$, which is akin to Na⁺ ions (1.02 Å) [111]. This may explain the comparable H⁺ and Na⁺ insertion potentials.

Protons also render an extremely high-rate capability in hydrous PBA electrodes. The most conspicuous attribute of protons is their superior ionic conductivity in aqueous electrolytes, which essentially stems from the unique Grotthuss

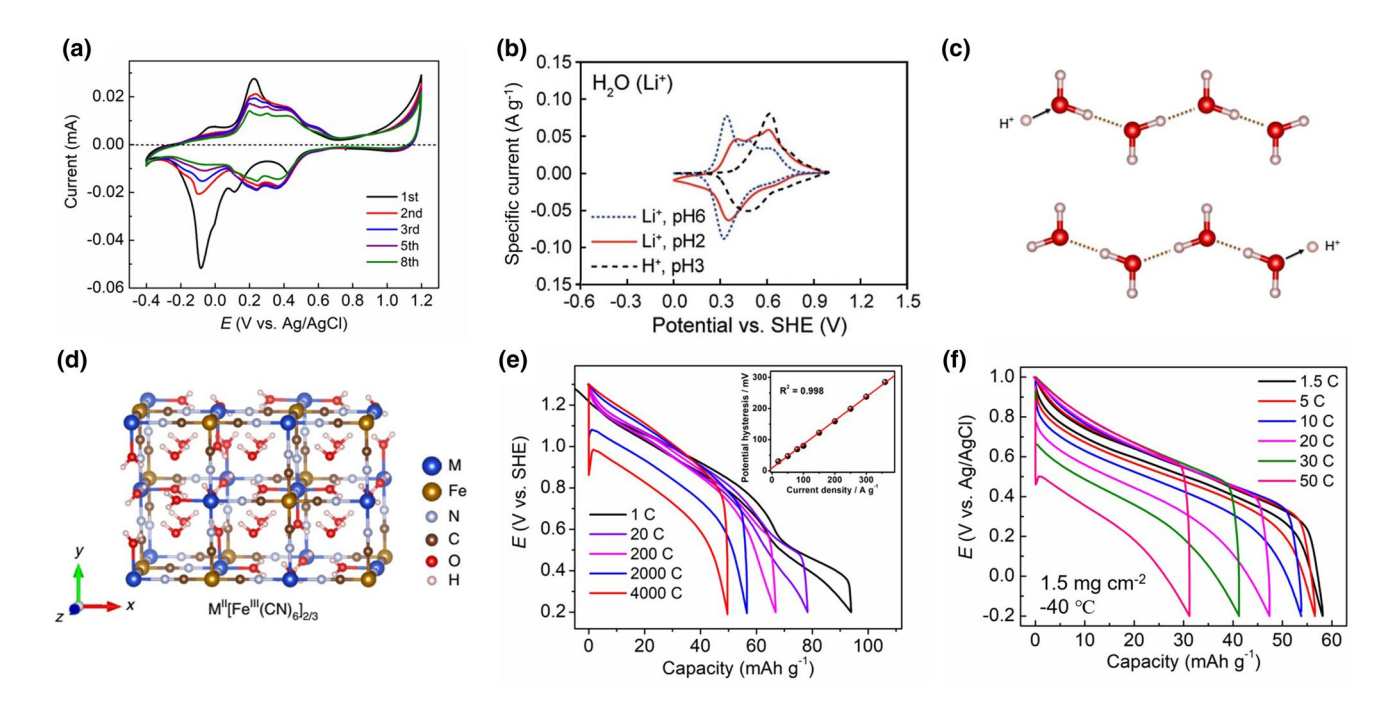


Fig. 8 a The CV curves of FeFe(CN)₆ in 0.1 M ${\rm H_2SO_4}$ electrolytes. **b** The CV curve comparison of NiFe-PBA for Li⁺ and H⁺ insertion. Reproduced with permission from Ref. [118]. Copyright 2014, The Royal Society of Chemistry. **c** The scheme of the Grotthuss mechanism. **d** The scheme of a defective TBA structure. **e** The rate capa-

bility of CuFe-TBA electrode. Reproduced with the permission from Ref. [123]. Copyright 2019, Springer Nature. **f** The low-temperature performance of the NiFe-TBA electrode. Reproduced with the permission from Ref. [124]. Copyright 2020, American Chemical Society



mechanism [121, 122]. A hydrogen-bounded water chain conducts protons by the cooperative bond re-arrangement of O-H covalent bonds and O···H hydrogen bonds, which results in the structural diffusion of protons (Fig. 8c) [123]. To utilize such a mechanism, our group recently designed a highly defective Turnbull's blue analogue (TBA) of $\text{Cu}[\text{Fe}(\text{CN})_6]_{0.63} \cdot \square_{0.37} \cdot 3.4 \text{H}_2\text{O}$, where ligand and zeolitic water molecules are concertedly connected to yield a contiguous hydrogen-bonding network (Fig. 8d) [123]. Based on the redox reactions of C-Fe^{III}/Fe^{II} and N-Cu^{II}/Cu^I couples, this electrode delivers a reasonable capacity of ~95 mAh g⁻¹, which corresponds to the storage of 0.91 mol protons per unit formula. Surprisingly, it delivers an unprecedented rate capability up to 4000 C with low-potential hysteresis (Fig. 8e) and record-long cycling stability of 0.73 million cycles, which surpasses the performance of storing any metal ions in PBA structures [123]. More importantly, the Grotthuss mechanism endows fascinating low-temperature performance in TBA electrodes. Figure 8f shows the charge/ discharge profiles of NiFe-TBA in 1.0 M H₂SO₄ electrolytes at -40 °C, where a high rate capability of 50 C is still attainable [124]. Recently, our group further disclosed that CuFe-TBA would deliver ~ 40% capacity utilization at a temperature of -78 °C in a 9.5 m H₃PO₄ electrolyte [125]. These studies showcase the power of the Grotthuss mechanism in revolutionizing fast insertion kinetics, which also extends the applicability of proton batteries in subzero temperature conditions.

However, there are some drawbacks for PBAs in aqueous proton batteries. Compared to the Na⁺, K⁺, and NH₄⁺ PWA versions, it is challenging to directly prepare the protoncontaining PWAs to assemble full cells, due to the instability of H₄Fe(CN)₆ precursors. To address this issue, our group has demonstrated the effectiveness of using hydrazine to chemically reduce the proton-deficient PBAs [123, 125]. For instance, we assembled a proton full cell based on the proton-bearing CuFe-PWA cathode and a MoO₃ anode, which demonstrates an energy density of 40 Wh kg⁻¹ (based on the active mass of two electrodes) and cycling retention of 85% after 1000 cycles [125]. Alternatively, it is viable to fabricate hybrid full cells based on the proton-deficient PBAs and metal anodes. Recently, Zhi et al. reported that copper metal could exhibit a stable plating/stripping reaction in the hybrid electrolyte of CuSO₄ and H₂SO₄ [126]. When paired with the CuFe-PBA cathode, this H⁺/Cu²⁺ hybrid full cell delivers an average voltage of ~0.7 V and outstanding cycling of 5000 cycles at a 20 C rate.

3 Discussions and Perspectives

From the description above, it is evident that the choice of ionic charge carriers greatly impacts the performance of PBA electrodes, including thermodynamics (capacity and potential), kinetics (the rate), and reversibility (structural compatibility and cycling) [45, 118]. For better visualization, we summarized the representative PBA performance for H⁺, Li⁺, Na⁺, K⁺, and NH₄⁺ storage in Table 2. We also draw a radar plot in Fig. 9a to compare the performance of monovalent ions in PBA electrodes.

Due to the intrinsic structural incompatibility between hydrated Li⁺ ions and PBA voids, PBAs are likely unsuitable for aqueous Li-ion batteries, which suffer from the serious capacity fading and low voltages [45, 60]. However, from the scientific research point of view, it would be interesting to investigate whether PBAs can show improved Li-insertion reversibility in WiS electrolytes, owing to their distinct hydration/solvation structures [47]. This aspect has remained unexplored to date. In comparison, PBAs demonstrate very promising performance in aqueous Na and K-ion batteries due to their overall reasonable capacity, voltage, rate, and cycling performance. Particularly, FeFe and MnFe-PBAs represent the leading materials in Na and K-ion batteries, considering the low toxicity and high abundance of Fe/Mn elements.

We also underline that PBAs promise the development of innovative non-metal ion batteries of $\rm H^+$ and $\rm NH_4^+$. Although some PBAs may dissolve in acidic electrolytes, the strategies of doping [69], material coating [31, 127], or utilizing WiS electrolytes [68, 128] will likely enhance the cycling stability. More importantly, the superior high-rate performance will be extremely appealing for fast-charging applications in grid-scale energy storage. On the other hand, $\rm NH_4^+$ insertion stands out by the overwhelmingly high potential and stable cycling, which compensate for the capacity drawbacks.

However, there are still some critical knowledge gaps and challenges for the applications of PBAs in aqueous batteries. Albeit the increasing reports of PBAs in rechargeable batteries, in-depth fundamental understanding about the comparative storage mechanism of different ions is still lacking. It has been widely suggested that FeFe, MnFe, and CoFe-PBAs are amenable to two-electron reactions for various ions [67, 102, 106]; however, it seems that only the ions that optimally match the PBA voids (Na⁺ and K⁺) can realize the highest capacity utilization (Fig. 9b). For instance, the FeFe(CN)₆ electrode delivers a specific capacity of ~100, 105, 120, 120, and 90 mAh g⁻¹ for H⁺, Li⁺, Na⁺, K⁺, and NH₄⁺ insertion, respectively, which suggests an inhibition effect of both small (H⁺ and Li⁺) and bulky (NH₄⁺) ions on the C-Fe^{III}/Fe^{II} redox couple (Fig. 9c). More interestingly,



 Table 2
 Electrode performance of PBA electrodes for various monovalent ions

Host	Material	Ion	Capacity (mAh g ⁻¹)	Potential (V vs. SHE)	C Rate/utilization	Cycle rate, cycle number and retention	Cycling time (day)
NiFe	Ni[Fe(CN) ₆] _{0.60} ·4.5H ₂ O [125]	H ⁺	~65	~0.65	6000 C, 50%	10 C, 1000, 73%	6.1
	K _{0.5} Ni[Fe(CN) ₆] _{0.83} ·3H ₂ O [45]	Li ⁺	~60	~0.50	41.7 C, 58%	8.3 C, 500, 40%	2.0
	K _{0.5} Ni[Fe(CN) ₆] _{0.83} ·3H ₂ O [62]	$Na^+ (pH=2)$	~60	~0.60	41.7 C, 66%	8.3 C, 5000, 100%	50
	K _{0.5} Ni[Fe(CN) ₆] _{0.83} ·3H ₂ O [62]	$K^+ (pH=2)$	~60	~0.70	41.7 C, 66%	8.3 C, 5000, 98%	49
	K_2 NiFe(CN) ₆ ·1.2H ₂ O [101]	K ⁺	~75	~0.80	500 C, 55%	30 C, 5000, 98.6%	13.9
	$K_{0.5}Ni[Fe(CN)_6]_{0.83} \cdot 3H_2O$ [45]	NH ₄ ⁺	~60	~0.75	41.7 C, 39%	8.3 C, 500, 88%	4.4
	(NH ₄) _{1.47} Ni[Fe(CN) ₆] _{0.88} [113]	NH ₄ ⁺	~60	~0.85	20 C, 50%	5.0 C, 2000, 74%	25
CuFe	Cu[Fe(CN) ₆] _{0.63} ·3.4H ₂ O [123]	H ⁺	~95	~0.85	4000 C, 50%	500 C, 730000, 60%	45
	$K_{0.7}Cu[Fe(CN)_6]_{0.77}$ [45]	Li ⁺	~60	~0.80	41.7 C, 65%	8.3 C, 500, 35%	1.75
	$K_{0.7}Cu[Fe(CN)_6]_{0.77}$ [45]	Na ⁺	~60	~0.90	41.7 C, 34%	8.3 C, 500, 77%	3.85
	$K_{0.7}Cu[Fe(CN)_6]_{0.77}$ [45]	K^+	~60	~1.0	41.7 C, 84%	8.3 C, 500, 99%	5.0
	K _{0.71} Cu[Fe(CN) ₆] _{0.72} ·3.7H ₂ O [63]	$K^+ (pH=2)$	~60	~1.0	83 C, 67%	17 C, 40000, 83%	154
	$K_{0.7}Cu[Fe(CN)_6]_{0.77}$ [45]	NH_4^+	~60	~1.05	41.7 C, 75%	8.3 C, 500, 91%	4.6
	$K_{0.72}$ Cu[Fe(CN) ₆] _{0.78} ·3.7H ₂ O [114]	NH ₄ ⁺	~60	~1.0	40 C, 83%	30 C, 1000, 78%	2.5
FeFe	Fe[Fe(CN) ₆] _{0.94} ·1.6H ₂ O [123]	H ⁺	~102	0.3 and 1.0	200 C, 48%	N/A	N/A
	Fe[Fe(CN) ₆] _{0.88} ·2.8H ₂ O	Li ⁺	~95	0.2 and 0.9	N/A	0.5 C, 15, 69%	1.75
	Fe[Fe(CN) ₆] _{0.88} ·2.8H ₂ O [44]	Na ⁺	~130	0.3 and 1.1	770 C, 50%	7.7 C, 1000, 72%	9.2
	Fe[Fe(CN) ₆] _{0.88} ·2.8H ₂ O [44]	K ⁺	~130	0.4 and 1.1	770 C, 50%	7.7 C, 1000, 48%	8.11
	K_2 FeFe(CN) ₆ ·2H ₂ O [104]	K ⁺	~120	0.4 and 1.1	25 C, 73%	4.2 C, 500, 96%	9.7
	Fe[Fe(CN) ₆] _{0.88} ·2.8H ₂ O [44]	NH ₄ ⁺	~90	0.45	1100 C, 45%	11 C, 4000, 88% (55 C, 50000, 78%)	28.8 (59)
MnFe	Mn[Fe(CN) ₆] _{0.67} · n H ₂ O [123]	H ⁺	~60	0.65	N/A	N/A	N/A
	Na _{1.24} Mn[Fe(CN) ₆] _{0.81} ·1.28H ₂ O [68]	Na ⁺ (WiS)	~116	0.8 and 1.3	N/A	0.22 C, 100, 43% (0.86 C, 100, 74%)	26.5 (8.43)
	K _{1.85} Fe _{0.33} Mn _{0.67} [Fe(CN) ₆] _{0.98} ·0.77H ₂ O [106]	K ⁺ (WiS)	~130	1.0 and 1.2	120 C, 65%	100 C, 10000, 90%	7.92
CoFe	$Co[Fe(CN)_6]_{0.67} \cdot nH_2O$ [123]	H ⁺	~60	0.7	N/A	N/A	N/A
	Na _{1.85} Co[Fe(CN) ₆] _{0.99} ·2.5H ₂ O [67]	Na ⁺	~128	0.6 and 1.1	20 C, 50%	5 C, 800, 91%	12.6
	K ₂ CoFe(CN) ₆ ·nH ₂ O	K ⁺	~47	0.6 and 0.95	N/A	2.2 C, 150, 61%	4.4

the Na⁺ ion insertion in Na₂CoFe(CN)₆ operates on a twoelectron reaction, whereas the K⁺ ions restrict the redox activity of both C-Fe^{III}/Fe^{II} and N-Co^{III}/Co^{II} redox couples (Fig. 9d). To unravel the correlation between ion charge carrier species and resulted capacity, a series of characterization on PBAs is indispensable to systematically learn the properties such as the crystal structures, electronic states, and the coordination environments [129–131].



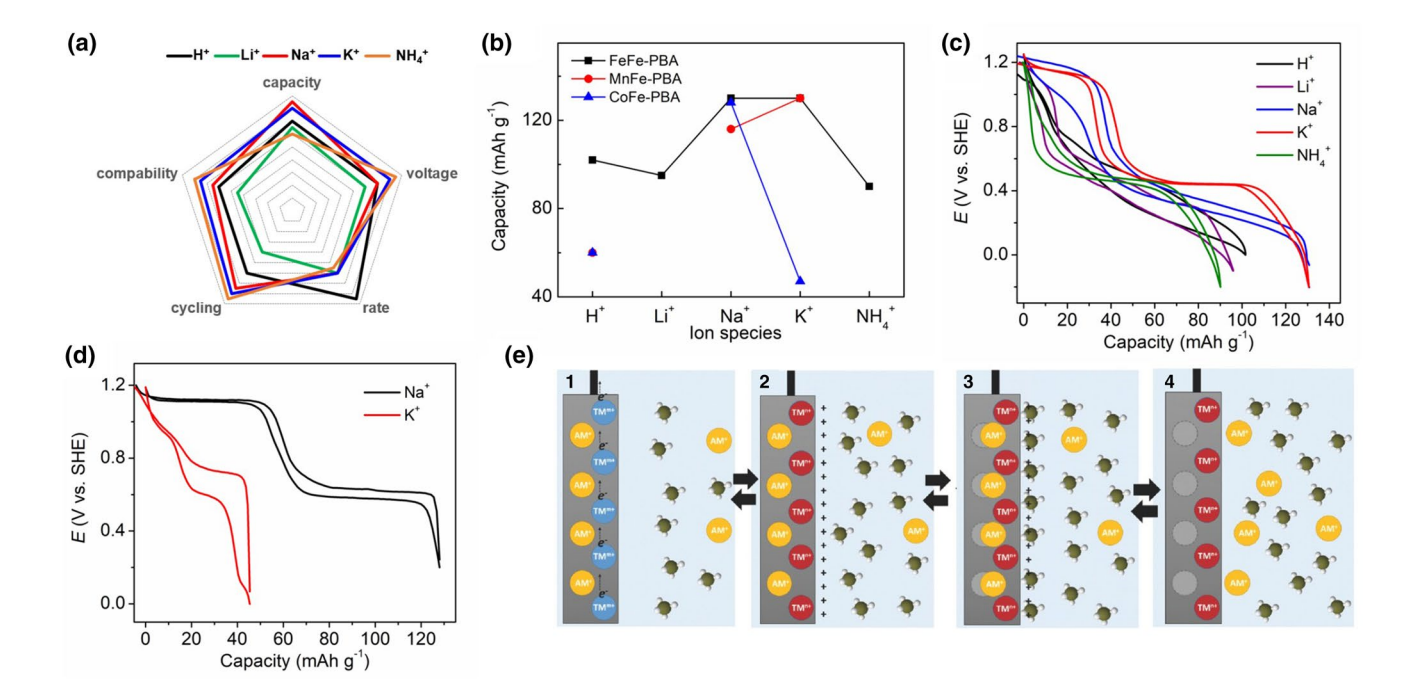


Fig. 9 a The radar plot of PBA electrodes for monovalent ion storage in aqueous electrolytes. b The influence of various ions on the reaction capacity of FeFe, MnFe, and Co-Fe PBAs. c The charge/discharge curve comparison of the BG electrode for different ions. d The charge/discharge curve comparison of the low-defect A₂CoFe(CN)₆

framework for Na⁺ and K⁺ insertion. **e** The scheme of the three-stage cation (de)insertion mechanism at the interface between PBA electrodes and aqueous electrolytes. The transition metal and alkali metal ions are abbreviated by TM^{m+} and AM⁺, respectively. Reproduced with the permission from Ref. [135]. Copyright 2016, Wiley–VCH

PBAs generally exhibit an outstanding rate capability of 40–4000 C (Table 2), which is an attractive merit for storage batteries. Such superb ion insertion kinetics primarily stems from the favourable 3D open channels of PBAs and the remarkably high ionic conductivity of aqueous electrolytes ($\sim 10^2$ S cm⁻¹) [5, 6]. Particularly, the interfacial understanding of PBA electrodes and aqueous electrolytes represents a crucial but intricate topic. In light of electrochemical quartz crystal microbalance (EQCM) studies on PBA thin films [132–134], smaller ions of Li⁺ and Na⁺ are perceived partially hydrated upon the entry into PBA voids, whereas larger ions of K⁺ and NH₄⁺ are inserted into the lattice in their naked forms with complete dehydration. This may be related to the fitness of naked or hydrated ions (Table 1) in PBA interstitial sites (Fig. 1). The dynamic ion migration across the electrode interface is associated with nuances. For instance, Bandarenka et al. have proposed a three-stage ion insertion mechanism for PBAs in aqueous Li⁺, Na⁺, and K⁺ systems [135, 136]. Due to the relatively fast electronic conduction but slower ionic conduction, transition metal ions in PBAs will get oxidized in the first place during charging (Fig. 9e, 1), whereas the jammed cation migration will lead to the presence of extra positive charges at the electrode surface (Fig. 9e, 2) [135]. As a result, the electrode will absorb some anions from electrolytes to temporarily compensate for the charge, which results in additional interfacial charge transfer (Fig. 9e, 3) [135]. Eventually, the monovalent ions will be extracted from the electrode, which progressively dismisses the accumulated anions at the interface (Fig. 9e, 4) [135]. Deep understanding of such dynamic processes will establish the correlation between the ion (cations, water molecules, and anions) migration manner and PBA reaction kinetics.

On the other hand, the excellent rate performance is also at the expense of sub-optimal electrode composition and active mass loading. Due to the moderate electronic conductivity of PBAs ($\sim 10^{-3} \text{ S cm}^{-1}$) [83], most studies have used massive amounts of carbon additives (10-20 wt%) and relatively low active mass loading $(1.5-10 \text{ mg cm}^{-2})$, which appreciably compromises the electrode capacity and area capacity. To have a better picture, we select some representative studies and list the electrode composition, active mass loading, and area capacity in Table 3, where most of them exhibit a low area capacity < 1 mAh cm⁻². In a stark contrast, commercial lithium-ion batteries have adopted a low content of carbon (e.g., 2 wt%) and binder (e.g., 2 wt%) at high active mass loading, e.g., 20 mg cm⁻², which results in a high area capacity of 4.0 mAh cm⁻² for the LiNi_{0.8}Mn_{0.1}Co_{0.1}O₂ and LiNi_{0.6}Mn_{0.2}Co_{0.2}O₂ cathodes [137]. We call for that future PBA studies may consider



Table 3 Electrode composition, mass loading, and area capacity information of some representative PBA studies

Material	Ion	Active material capacity (mAh g ⁻¹)	Conducting carbon and binder (wt%)	Electrode capacity (mAh g ⁻¹)	Active mass loading (mg cm ⁻²)	Electrode area capacity (mAh cm ⁻²)
NiFe-PBAs [45]	Na ⁺	60	11 and 9	48	10	~0.60
NiFe-PBAs [101]	K^+	75	20 and 10	53	~2	~0.15
CuFe-PBAs [65]	Na ⁺	60	20 and 10	42	10	~0.60
CuFe-PBAs [45]	K^+	60	11 and 9	48	10	~0.60
CuFe-PBAs [123]	H^+	95	20 and 10	67	1.5	~0.14
FeFe-PBAs [44]	Na ⁺	130	20 and 10	91	1.5	~0.195
FeFe-PBAs [104]	K^+	120	10 and 10	96	2.0	~0.24
FeFe-PBAs [44]	NH_4^+	90	20 and 10	63	1.5	~0.135
CoFe-PBAs [84]	Na ⁺	110	20 and 10	77	6.4	~0.70
MnFe-PBAs [68]	Na ⁺	120	25 and 5	72	20	~2.4
MnFe-PBAs [93]	K^+	130	20 and 10	91	5.8	~0.75

the optimization of electrode composition or PBA/carbon microstructure configuration, such as in situ hybridization with conducting carbon or polymers [138], which helps to increase the electronic conductivity and mass loading [139].

Another hurdle for PBAs is their often-short cycling life. We note that the cycling life of electrodes in aqueous batteries should be characterized by both the number of cycles (n) and cycling time (hours, days, etc.) [140]. Apparently, the one-electron reaction of NiFe and CuFe-PBAs renders larger cycling numbers of 2000-730000, whereas the twoelectron reaction of FeFe and MnFe-PBAs shows fewer numbers of 500–1000 cycles (Table 2). However, NiFe and CuFe-PBAs comprise relatively more expensive Ni and Cu elements, which may not be affordable for large-scale utilization. Besides, their moderate capacity of ~ 60 mAh g⁻¹ will restrict the energy density, which underlines the importance of high-capacity FeFe and MnFe-PBA electrodes. However, the cycling of 500-1000 cycles is insufficient for practical applications of stationary storage. On the other hand, the cycling time of PBAs is also unsatisfactory. Due to the lack of a stable solid-electrolyte interphase (SEI), aqueous electrolytes are subject to severer side reactions such as water electrolysis or local pH changes [17]. To combat this shortcoming, a common tactic is to use high current rates to "mask" side reactions or material dissolution [141], which generally renders larger cycling numbers. However, if we consider the cycling time, most PBA electrodes show a short calendar life of < 30 days (Table 2). Although adding some acids can facilitate the cycling stability, it significantly increases the corrosion to current collectors and restricts the choice of anode materials. The use of concentrated electrolytes is also conducive to increase the calendar life; however, it brings about other issues such as the increased electrolyte viscosity, difficult wetting, and higher cell cost [142]. Based on these considerations, we advocate scrutinizing the capacity fading mechanism of PBA materials in aqueous electrolytes, which are essentially insoluble precipitates with stable crystal structures.

In summary, we introduced the research progress of PBA materials in aqueous monovalent ion batteries and shared some insights on the knowledge gaps of these materials. Due to their fascinating redox chemistry, simple synthesis, and potentially low cost, PBAs represent a class of coordination compounds that hold a great promise for aqueous H⁺, Na⁺, K⁺, and NH₄⁺ batteries. However, the reported performance is still insufficient for practical applications, and the underlying reaction mechanisms, such as correlations of ion-electrode capacity and the capacity fading as a function of ion charge carriers, remain inconclusive. To facilitate the applications of PBAs in practical aqueous batteries, future studies may focus on the fundamental understanding of the ion storage mechanisms and the demonstration of highcapacity and long-life FeFe and MnFe-PBA materials in more practical conditions.

Acknowledgements X. Ji thanks the financial support from U.S. National Science Foundation Award No. DMR 2004636.

Compliance with Ethical Standards

Conflict of interest The authors declared that they have no conflict of interest.

References

Yang, Z.G., Zhang, J.L., Kintner-Meyer, M.C.W., et al.: Electrochemical energy storage for green grid. Chem. Rev. 111, 3577–3613 (2011). https://doi.org/10.1021/cr100290v



- Goodenough, J.B., Park, K.S.: The Li-ion rechargeable battery: a perspective. J. Am. Chem. Soc. 135, 1167–1176 (2013). https://doi.org/10.1021/ja3091438
- Cao, Y.L., Xiao, L.F., Sushko, M.L., et al.: Sodium ion insertion in hollow carbon nanowires for battery applications. Nano Lett. 12, 3783–3787 (2012). https://doi.org/10.1021/nl3016957
- Ji, X.L.: A paradigm of storage batteries. Energy Environ. Sci. 12, 3203–3224 (2019). https://doi.org/10.1039/c9ee02356a
- Bin, D., Wang, F., Tamirat, A.G., et al.: Progress in aqueous rechargeable sodium-ion batteries. Adv. Energy Mater. 8, 1703008 (2018). https://doi.org/10.1002/aenm.201703008
- Chao, D.L., Zhou, W.H., Xie, F.X., et al.: Roadmap for advanced aqueous batteries: from design of materials to applications. Sci. Adv. 6, eaba4098 (2020). https://doi.org/10.1126/sciadv.aba4098
- Gao, X.Y., Zhang, H.Z., Liu, X.Q., et al.: Flexible Zn-ion batteries based on manganese oxides: progress and prospect. Carbon Energy 2, 387–407 (2020). https://doi.org/10.1002/cey2.63
- Lai, C.S., McCulloch, M.D.: Levelized cost of electricity for solar photovoltaic and electrical energy storage. Appl. Energy 190, 191–203 (2017). https://doi.org/10.1016/j.apenergy.2016.12.153
- Li, W., Dahn, J.R., Wainwright, D.S.: Rechargeable lithium batteries with aqueous electrolytes. Science 264, 1115–1118 (1994). https://doi.org/10.1126/science.264.5162.1115
- Li, Z., Young, D., Xiang, K., et al.: Towards high power high energy aqueous sodium-ion batteries: the NaTi₂(PO₄)₃/ Na_{0.44}MnO₂ system. Adv. Energy Mater. 3, 290–294 (2013). https://doi.org/10.1002/aenm.201200598
- Pasta, M., Wessells, C.D., Huggins, R.A., et al.: A high-rate and long cycle life aqueous electrolyte battery for grid-scale energy storage. Nat. Commun. 3, 1–7 (2012). https://doi.org/10.1038/ ncomms2139
- Dong, S.Y., Shin, W., Jiang, H., et al.: Ultra-fast NH₄⁺ storage: strong h bonding between NH₄⁺ and bi-layered V₂O₅. Chem 5, 1537–1551 (2019). https://doi.org/10.1016/j.chempr.2019.03.009
- Chen, L., Bao, J.L., Dong, X., et al.: Aqueous Mg-ion battery based on polyimide anode and Prussian blue cathode. ACS Energy Lett. 2, 1115–1121 (2017). https://doi.org/10.1021/acsen ergylett.7b00040
- Gheytani, S., Liang, Y.L., Wu, F.L., et al.: An aqueous Ca-ion battery. Adv. Sci. 4, 1700465 (2017). https://doi.org/10.1002/ advs.201700465
- Wang, P.J., Shi, X.D., Wu, Z.X., et al.: Layered hydrated vanadium oxide as highly reversible intercalation cathode for aqueous Zn-ion batteries. Carbon Energy 2, 294–301 (2020). https://doi. org/10.1002/cey2.39
- Li, Z., Xiang, K., Xing, W.T., et al.: Reversible aluminum-ion intercalation in Prussian blue analogs and demonstration of a high-power aluminum-ion asymmetric capacitor. Adv. Energy Mater. 5, 1401410 (2015). https://doi.org/10.1002/aenm.20140
- Suo, L.M., Borodin, O., Gao, T., et al.: "Water-in-salt" electrolyte enables high-voltage aqueous lithium-ion chemistries. Science 350, 938–943 (2015). https://doi.org/10.1126/science.aab1595
- Kim, H., Hong, J., Park, K.Y., et al.: Aqueous rechargeable Li and Na ion batteries. Chem. Rev. 114, 11788–11827 (2014). https://doi.org/10.1021/cr500232y
- Wang, Y.S., Liu, J., Lee, B., et al.: Ti-substituted tunnel-type Na_{0.44}MnO₂ oxide as a negative electrode for aqueous sodium-ion batteries. Nat. Commun. 6, 1–10 (2015). https://doi.org/10.1038/ ncomms7401
- Whitacre, J.F., Tevar, A., Sharma, S.: Na₄Mn₉O₁₈ as a positive electrode material for an aqueous electrolyte sodium-ion energy storage device. Electrochem. Commun. 12, 463–466 (2010). https://doi.org/10.1016/j.elecom.2010.01.020
- 21. Park, S.I., Gocheva, I., Okada, S., et al.: Electrochemical properties of $NaTi_2(PO_4)_3$ anode for rechargeable aqueous sodium-ion

- batteries. J. Electrochem. Soc. **158**, A1067 (2011). https://doi.org/10.1149/1.3611434
- 22. Qiu, S., Wu, X.Y., Wang, M.Y., et al.: NASICON-type Na₃Fe₂(PO₄)₃ as a low-cost and high-rate anode material for aqueous sodium-ion batteries. Nano Energy **64**, 103941 (2019). https://doi.org/10.1016/j.nanoen.2019.103941
- Zhang, Y.D., An, Y.F., Yin, B., et al.: A novel aqueous ammonium dual-ion battery based on organic polymers. J. Mater. Chem. A 7, 11314–11320 (2019). https://doi.org/10.1039/c9ta00254e
- Luo, J.Y., Xia, Y.Y.: Aqueous lithium-ion battery LiTi₂(PO₄)₃/ LiMn₂O₄ with high power and energy densities as well as superior cycling stability. Adv. Funct. Mater. 17, 3877–3884 (2007). https://doi.org/10.1002/adfm.200700638
- Masquelier, C., Croguennec, L.: Polyanionic (phosphates, silicates, sulfates) frameworks as electrode materials for rechargeable Li (or Na) batteries. Chem. Rev. 113, 6552–6591 (2013). https://doi.org/10.1021/cr3001862
- Nevers, D.R., Brushett, F.R., Wheeler, D.R.: Engineering radical polymer electrodes for electrochemical energy storage. J. Power Sources 352, 226–244 (2017). https://doi.org/10.1016/j.jpows our.2017.03.077
- Eftekhari, A.: Potassium secondary cell based on Prussian blue cathode. J. Power Sources 126, 221–228 (2004). https://doi. org/10.1016/j.jpowsour.2003.08.007
- 28. Luo, J.H., Sun, S.X., Peng, J., et al.: Graphene-roll-wrapped Prussian blue nanospheres as a high-performance binder-free cathode for sodium-ion batteries. ACS Appl. Mater. Interfaces 9, 25317–25322 (2017). https://doi.org/10.1021/acsami.7b06334
- 29. Wu, X.Y., Shao, M.M., Wu, C.H., et al.: Low defect FeFe(CN)₆ framework as stable host material for high performance Li-ion batteries. ACS Appl. Mater. Interfaces **8**, 23706–23712 (2016). https://doi.org/10.1021/acsami.6b06880
- Asakura, D., Okubo, M., Mizuno, Y., et al.: Fabrication of a cyanide-bridged coordination polymer electrode for enhanced electrochemical ion storage ability. J. Phys. Chem. C 116, 8364– 8369 (2012). https://doi.org/10.1021/jp2118949
- Asakura, D., Li, C.H., Mizuno, Y., et al.: Bimetallic cyanide-bridged coordination polymers as lithium ion cathode materials: core@shell nanoparticles with enhanced cyclability. J. Am. Chem. Soc. 135, 2793–2799 (2013). https://doi.org/10.1021/ja312160v
- Pasta, M., Wessells, C.D., Liu, N., et al.: Full open-framework batteries for stationary energy storage. Nat. Commun. 5, 1–9 (2014). https://doi.org/10.1038/ncomms4007
- Wang, L., Song, J., Qiao, R.M., et al.: Rhombohedral Prussian white as cathode for rechargeable sodium-ion batteries. J. Am. Chem. Soc. 137, 2548–2554 (2015). https://doi.org/10.1021/ja510347s
- You, Y., Wu, X.L., Yin, Y.X., et al.: A zero-strain insertion cathode material of nickel ferricyanide for sodium-ion batteries. J. Mater. Chem. A 1, 14061 (2013). https://doi.org/10.1039/c3ta13223d
- Wu, X.Y., Deng, W.W., Qian, J.F., et al.: Single-crystal FeFe(CN)₆ nanoparticles: a high capacity and high rate cathode for Na-ion batteries. J. Mater. Chem. A 1, 10130 (2013). https:// doi.org/10.1039/c3ta12036h
- Imanishi, N., Morikawa, T., Kondo, J., et al.: Lithium intercalation behavior into iron cyanide complex as positive electrode of lithium secondary battery. J. Power Sources 79, 215–219 (1999). https://doi.org/10.1016/s0378-7753(99)00061-0
- Jiang, Y.Z., Yu, S.L., Wang, B.Q., et al.: Prussian blue@C composite as an ultrahigh-rate and long-life sodium-ion battery cathode. Adv. Funct. Mater. 26, 5315–5321 (2016). https://doi.org/10.1002/adfm.201600747



- Liu, Q.N., Hu, Z., Chen, M.Z., et al.: The cathode choice for commercialization of sodium-ion batteries: layered transition metal oxides versus Prussian blue analogs. Adv. Funct. Mater. 30, 1909530 (2020). https://doi.org/10.1002/adfm.201909530
- Goda, E.S., Lee, S., Sohail, M., et al.: Prussian blue and its analogues as advanced supercapacitor electrodes. J. Energy Chem. 50, 206–229 (2020). https://doi.org/10.1016/j.jeche m.2020.03.031
- Rajagopalan, R., Tang, Y.G., Ji, X.B., et al.: Advancements and challenges in potassium ion batteries: a comprehensive review. Adv. Funct. Mater. 30, 1909486 (2020). https://doi.org/10.1002/ adfm.201909486
- Lee, H.W., Wang, R.Y., Pasta, M., et al.: Manganese hexacyanomanganate open framework as a high-capacity positive electrode material for sodium-ion batteries. Nat. Commun. 5, 1–6 (2014). https://doi.org/10.1038/ncomms6280
- Xiao, B.W.: Intercalated water in aqueous batteries. Carbon Energy 2, 251–264 (2020). https://doi.org/10.1002/cey2.55
- Tansel, B.: Significance of thermodynamic and physical characteristics on permeation of ions during membrane separation: hydrated radius, hydration free energy and viscous effects. Sep. Purif. Technol. 86, 119–126 (2012). https://doi.org/10.1016/j.seppur.2011.10.033
- 44. Wu, X.Y., Xu, Y.K., Jiang, H., et al.: NH₄⁺ topotactic insertion in berlin green: an exceptionally long-cycling cathode in aqueous ammonium-ion batteries. ACS Appl. Energy Mater. 1, 3077–3083 (2018). https://doi.org/10.1021/acsaem.8b00789
- Wessells, C.D., Peddada, S.V., McDowell, M.T., et al.: The effect of insertion species on nanostructured open framework hexacyanoferrate battery electrodes. J. Electrochem. Soc. 159, A98–A103 (2011). https://doi.org/10.1149/2.060202jes
- Wang, R.Y., Wessells, C.D., Huggins, R.A., et al.: Highly reversible open framework nanoscale electrodes for divalent ion batteries. Nano Lett. 13, 5748–5752 (2013). https://doi. org/10.1021/nl403669a
- Zhou, A.X., Jiang, L.W., Yue, J.M., et al.: Water-in-salt electrolyte promotes high-capacity FeFe(CN)₆ cathode for aqueous Al-ion battery. ACS Appl. Mater. Interfaces 11, 41356–41362 (2019). https://doi.org/10.1021/acsami.9b14149
- 48. Yang, Q., Mo, F.N., Liu, Z.X., et al.: Activating C-coordinated iron of iron hexacyanoferrate for Zn hybrid-ion batteries with 10,000-cycle lifespan and superior rate capability. Adv. Mater. (2019). https://doi.org/10.1002/adma.201901521
- 49. Wu, X.Y., Markir, A., Xu, Y.K., et al.: A rechargeable battery with an iron metal anode. Adv. Funct. Mater. 29, 1900911 (2019). https://doi.org/10.1002/adfm.201900911
- Wang, R.Y., Shyam, B., Stone, K.H., et al.: Reversible multivalent (monovalent, divalent, trivalent) ion insertion in open framework materials. Adv. Energy Mater. 5, 1401869 (2015). https://doi.org/10.1002/aenm.201401869
- Guo, X.Y., Wang, Z.B., Deng, Z., et al.: Water contributes to higher energy density and cycling stability of Prussian blue analogue cathodes for aqueous sodium-ion batteries. Chem. Mater. 31, 5933–5942 (2019). https://doi.org/10.1021/acs. chemmater.9b02269
- Neff, V.D.: Electrochemical oxidation and reduction of thin films of Prussian blue. J. Electrochem. Soc. 125, 886–887 (1978). https://doi.org/10.1149/1.2131575
- Ellis, D., Eckhoff, M., Neff, V.D.: Electrochromism in the mixed-valence hexacyanides. 1. Voltammetric and spectral studies of the oxidation and reduction of thin films of Prussian blue. J. Phys. Chem. 85, 1225–1231 (1981). https://doi. org/10.1021/j150609a026
- Itaya, K., Ataka, T., Toshima, S.: Spectroelectrochemistry and electrochemical preparation method of Prussian blue modified

- electrodes. J. Am. Chem. Soc. **104**, 4767–4772 (1982). https://doi.org/10.1021/ja00382a006
- Itaya, K., Uchida, I., Neff, V.D.: Electrochemistry of polynuclear transition metal cyanides: Prussian blue and its analogues. Acc. Chem. Res. 19, 162–168 (1986). https://doi.org/10.1021/ar00126a001
- 56. Karyakin, A.A.: Prussian blue and its analogues: electrochemistry and analytical applications. Electroanalysis **13**, 813–819 (2001). https://doi.org/10.1002/1521-4109(200106)13:10813:aid-elan813%3e3.0.co;2-z
- Scholz, F., Dostal, A.: The formal potentials of solid metal hexacyanometalates. Angew. Chem. Int. Ed. Engl. 34, 2685–2687 (1996). https://doi.org/10.1002/anie.199526851
- Yang, C., Chen, J., Ji, X., et al.: Aqueous Li-ion battery enabled by halogen conversion-intercalation chemistry in graphite. Nature 569, 245–250 (2019). https://doi.org/10.1038/s41586-019-1175-6
- Yang, C.Y., Suo, L.M., Borodin, O., et al.: Unique aqueous Li-ion/sulfur chemistry with high energy density and reversibility. Proc. Natl. Acad. Sci. 114, 6197–6202 (2017). https:// doi.org/10.1073/pnas.1703937114
- Yang, Q., Wang, W., Li, H., et al.: Investigation of iron hexacyanoferrate as a high rate cathode for aqueous batteries: sodiumion batteries and lithium-ion batteries. Electrochim. Acta 270, 96–103 (2018). https://doi.org/10.1016/j.electacta.2018.02.171
- Ling, C., Chen, J.J., Mizuno, F.: First-principles study of alkali and alkaline earth ion intercalation in iron hexacyanoferrate: the important role of ionic radius. J. Phys. Chem. C 117, 21158– 21165 (2013). https://doi.org/10.1021/jp4078689
- 62. Wessells, C.D., Peddada, S.V., Huggins, R.A., et al.: Nickel hexacyanoferrate nanoparticle electrodes for aqueous sodium and potassium ion batteries. Nano Lett. **11**, 5421–5425 (2011). https://doi.org/10.1021/nl203193q
- 63. Wu, X.Y., Cao, Y.L., Ai, X.P., et al.: A low-cost and environmentally benign aqueous rechargeable sodium-ion battery based on NaTi₂(PO₄)₃–Na₂NiFe(CN)₆ intercalation chemistry. Electrochem. Commun. 31, 145–148 (2013). https://doi.org/10.1016/j.elecom.2013.03.013
- Wessells, C.D., Huggins, R.A., Cui, Y.: Copper hexacyanoferrate battery electrodes with long cycle life and high power. Nat. Commun. 2, 550 (2011). https://doi.org/10.1038/ncomms1563
- Wu, X.Y., Sun, M.Y., Shen, Y.F., et al.: Energetic aqueous rechargeable sodium-ion battery based on Na₂CuFe(CN)₆-NaTi₂ (PO₄)₃ intercalation chemistry. ChemSusChem 7, 407–411 (2014). https://doi.org/10.1002/cssc.201301036
- 66. Fernández-Ropero, A.J., Piernas-Muñoz, M.J., Castillo-Martínez, E., et al.: Electrochemical characterization of NaFe₂(CN)₆ Prussian blue as positive electrode for aqueous sodium-ion batteries. Electrochim. Acta 210, 352–357 (2016). https://doi.org/10.1016/j.electacta.2016.05.176
- 67. Wu, X.Y., Sun, M.Y., Guo, S.M., et al.: Vacancy-free Prussian blue nanocrystals with high capacity and superior cyclability for aqueous sodium-ion batteries. ChemNanoMat 1, 188–193 (2015). https://doi.org/10.1002/cnma.201500021
- Nakamoto, K., Sakamoto, R., Ito, M., et al.: Effect of concentrated electrolyte on aqueous sodium-ion battery with sodium manganese hexacyanoferrate cathode. Electrochemistry 85, 179–185 (2017). https://doi.org/10.5796/electrochemistry.85.179
- Wessells, C.D., McDowell, M.T., Peddada, S.V., et al.: Tunable reaction potentials in open framework nanoparticle battery electrodes for grid-scale energy storage. ACS Nano 6, 1688–1694 (2012). https://doi.org/10.1021/nn204666v
- Wang, J., Mi, C.H., Nie, P., et al.: Sodium-rich iron hexacyanoferrate with nickel doping as a high performance cathode for aqueous sodium ion batteries. J. Electroanal. Chem. 818, 10–18 (2018). https://doi.org/10.1016/j.jelechem.2018.04.011



- Li, W.F., Zhang, F., Xiang, X.D., et al.: Electrochemical properties and redox mechanism of Na₂Ni_{0.4}Co_{0.6}[Fe(CN)₆] nanocrystallites as high-capacity cathode for aqueous sodium-ion batteries. J. Phys. Chem. C 121, 27805–27812 (2017). https://doi.org/10.1021/acs.jpcc.7b07920
- Wu, X.Y., Luo, Y., Sun, M.Y., et al.: Low-defect Prussian blue nanocubes as high capacity and long life cathodes for aqueous Na-ion batteries. Nano Energy 13, 117–123 (2015). https://doi. org/10.1016/j.nanoen.2015.02.006
- Wu, X.Y., Wu, C.H., Wei, C.X., et al.: Highly crystallized Na₂CoFe(CN)₆ with suppressed lattice defects as superior cathode material for sodium-ion batteries. ACS Appl. Mater. Interfaces 8, 5393–5399 (2016). https://doi.org/10.1021/acsami.5b126 20
- Lu, Y.H., Wang, L., Cheng, J.G., et al.: Prussian blue: a new framework of electrode materials for sodium batteries. Chem. Commun. 48, 6544 (2012). https://doi.org/10.1039/c2cc31777j
- Azhar, A., Li, Y.C., Cai, Z.X., et al.: Nanoarchitectonics: a new materials horizon for Prussian blue and its analogues. Bull. Chem. Soc. Jpn. 92, 875–904 (2019). https://doi.org/10.1246/ bcsj.20180368
- Li, W.J., Han, C., Cheng, G., et al.: Chemical properties, structural properties, and energy storage applications of Prussian blue analogues. Small 15, e1900470 (2019). https://doi.org/10.1002/smll.201900470
- de Wet, J.F., Rolle, R.: On the existence and Autoreduction of Iron(III)-hexacyanoferrate(III). Z. Anorg. Allg. Chem. 336, 96–103 (1965). https://doi.org/10.1002/zaac.19653360114
- 78. Walker, R.G., Watkins, K.O.: Kinetics of complex formation between hexacyanoferrate(III) ions and iron(III) to form FeFe(CN)₆ (Prussian brown). Inorg. Chem. **7**, 885–888 (1968). https://doi.org/10.1021/ic50063a009
- Kumar, A., Yusuf, S.M., Keller, L.: Structural and magnetic properties ofFe[Fe(CN)₆]·4H₂O. Phys. Rev. B 71, 054414 (2005). https://doi.org/10.1103/physrevb.71.054414
- Buser, H.J., Ludi, A., Petter, W., et al.: Single-crystal study of Prussian blue: Fe₄[Fe(CN)₆]₃·14H₂O. J. Chem. Soc. Chem. Commun. (1972). https://doi.org/10.1039/c39720001299
- 81. You, Y., Wu, X.L., Yin, Y.X., et al.: High-quality Prussian blue crystals as superior cathode materials for room-temperature sodium-ion batteries. Energy Environ. Sci. 7, 1643–1647 (2014). https://doi.org/10.1039/c3ee44004d
- Hu, M., Ishihara, S., Ariga, K., et al.: Kinetically controlled crystallization for synthesis of monodispersed coordination polymer nanocubes and their self-assembly to periodic arrangements. Chem. Eur. J. 19, 1882–1885 (2013). https://doi.org/10.1002/chem.201203138
- Liu, Y., Qiao, Y., Zhang, W.X., et al.: Sodium storage in Na-rich Na_xFeFe(CN)₆ nanocubes. Nano Energy 12, 386–393 (2015). https://doi.org/10.1016/j.nanoen.2015.01.012
- Shao, T.L., Li, C., Liu, C.Y., et al.: Electrolyte regulation enhances the stability of Prussian blue analogues in aqueous Na-ion storage. J. Mater. Chem. A 7, 1749–1755 (2019). https:// doi.org/10.1039/c8ta10860a
- Xu, L., Li, H., Wu, X.Y., et al.: Well-defined Na₂Zn₃[Fe(CN)₆]₂ nanocrystals as a low-cost and cycle-stable cathode material for Na-ion batteries. Electrochem. Commun. 98, 78–81 (2019). https://doi.org/10.1016/j.elecom.2018.11.019
- Peng, J., Wang, J.S., Yi, H.C., et al.: A dual-insertion type sodium-ion full cell based on high-quality ternary-metal Prussian blue analogs. Adv. Energy Mater. 8, 1702856 (2018). https://doi.org/10.1002/aenm.201702856
- 87. Yan, C.X., Zhao, A.L., Zhong, F.P., et al.: A low-defect and Na-enriched Prussian blue lattice with ultralong cycle life for sodium-ion battery cathode. Electrochim. Acta **332**, 135533 (2020). https://doi.org/10.1016/j.electacta.2019.135533

- Xu, Y., Wan, J., Huang, L., et al.: Dual redox-active copper hexacyanoferrate nanosheets as cathode materials for advanced sodium-ion batteries. Energy Storage Mater. 33, 432–441 (2020). https://doi.org/10.1016/j.ensm.2020.08.008
- Song, J., Wang, L., Lu, Y.H., et al.: Removal of interstitial H₂O in hexacyanometallates for a superior cathode of a sodium-ion battery. J. Am. Chem. Soc. 137, 2658–2664 (2015). https://doi.org/10.1021/ja512383b
- Li, W.J., Chou, S.L., Wang, J.Z., et al.: Multifunctional conducing polymer coated Na_{1+x}MnFe(CN)₆ cathode for sodium-ion batteries with superior performance via a facile and one-step chemistry approach. Nano Energy 13, 200–207 (2015). https://doi.org/10.1016/j.nanoen.2015.02.019
- 91. Nakamoto, K., Sakamoto, R., Sawada, Y., et al.: Prussian blue-type electrodes: over 2 V aqueous sodium-ion battery with Prussian blue-type electrodes. Small Methods **3**, 1970010 (2019). https://doi.org/10.1002/smtd.201970010
- Han, J., Zhang, H., Varzi, A., et al.: Fluorine-free water-in-salt electrolyte for green and low-cost aqueous sodium-ion batteries. ChemSusChem 11, 3704–3707 (2018). https://doi.org/10.1002/ cssc.201801930
- Jiang, L.W., Liu, L.L., Yue, J.M., et al.: High-voltage aqueous Na-ion battery enabled by inert-cation-assisted water-in-salt electrolyte. Adv. Mater. 32, 1904427 (2020). https://doi.org/10.1002/adma.201904427
- Betz, J., Bieker, G., Meister, P., et al.: Theoretical versus practical energy: a plea for more transparency in the energy calculation of different rechargeable battery systems. Adv. Energy Mater. 9, 1803170 (2019). https://doi.org/10.1002/aenm.201803170
- Paulitsch, B., Yun, J., Bandarenka, A.S.: Electrodeposited Na₂VO_x[Fe(CN)₆] films as a cathode material for aqueous Naion batteries. ACS Appl. Mater. Inter. 9, 8107–8112 (2017). https://doi.org/10.1021/acsami.6b15666
- 96. Shao, M.M., Wang, B., Liu, M.C., et al.: A high-voltage and cycle stable aqueous rechargeable Na-ion battery based on Na₂Zn₃[Fe(CN)₆]₂-NaTi₂(PO₄)₃ intercalation chemistry. ACS Appl. Energy Mater. 2, 5809–5815 (2019). https://doi.org/10.1021/acsaem.9b00935
- Chen, L., Zhang, L.Y., Zhou, X.F., et al.: Aqueous batteries based on mixed monovalence metal ions: a new battery family. ChemSusChem 7, 2295–2302 (2014). https://doi.org/10.1002/ cssc.201402084
- Lee, J.H., Ali, G., Kim, D.H., et al.: Metal-organic framework cathodes based on a vanadium hexacyanoferrate Prussian blue analogue for high-performance aqueous rechargeable batteries. Adv. Energy Mater. 7, 1601491 (2017). https://doi.org/10.1002/ aenm.201601491
- Chen, H., Zhang, Z., Wei, Z., et al.: Use of a water-in-salt electrolyte to avoid organic material dissolution and enhance the kinetics of aqueous potassium ion batteries. Sustain. Energy Fuels 4, 128–131 (2020)
- Leonard, D.P., Wei, Z.X., Chen, G., et al.: Water-in-salt electrolyte for potassium-ion batteries. ACS Energy Lett. 3, 373–374 (2018). https://doi.org/10.1021/acsenergylett.8b00009
- Ren, W.H., Chen, X.J., Zhao, C.: Ultrafast aqueous potassium-ion batteries cathode for stable intermittent grid-scale energy storage. Adv. Energy Mater. 8, 1801413 (2018). https://doi.org/10.1002/ aenm.201801413
- Bie, X.F., Kubota, K., Hosaka, T., et al.: A novel K-ion battery: hexacyanoferrate(ii)/graphite cell. J. Mater. Chem. A 5, 4325– 4330 (2017). https://doi.org/10.1039/c7ta00220c
- 103. Phadke, S., Mysyk, R., Anouti, M.: Effect of cation (Li⁺, Na⁺, K⁺, Rb⁺, Cs⁺) in aqueous electrolyte on the electrochemical redox of Prussian blue analogue (PBA) cathodes. J. Energy Chem. 40, 31–38 (2020). https://doi.org/10.1016/j.jechem.2019.01.025



- Su, D.W., McDonagh, A., Qiao, S.Z., et al.: High-capacity aqueous potassium-ion batteries for large-scale energy storage. Adv. Mater. 29, 1604007 (2017). https://doi.org/10.1002/adma.201604007
- 105. He, G., Nazar, L.F.: Crystallite size control of Prussian white analogues for nonaqueous potassium-ion batteries. ACS Energy Lett. 2, 1122–1127 (2017). https://doi.org/10.1021/acsenergyl ett.7b00179
- Jiang, L.W., Lu, Y.X., Zhao, C.L., et al.: Building aqueous K-ion batteries for energy storage. Nat. Energy 4, 495–503 (2019). https://doi.org/10.1038/s41560-019-0388-0
- Wu, X.Y., Jian, Z.L., Li, Z.F., et al.: Prussian white analogues as promising cathode for non-aqueous potassium-ion batteries. Electrochem. Commun. 77, 54–57 (2017). https://doi. org/10.1016/j.elecom.2017.02.012
- Matsuda, T., Kim, J., Moritomo, Y.: Symmetry switch of cobalt ferrocyanide framework by alkaline cation exchange. J. Am. Chem. Soc. 132, 12206–12207 (2010). https://doi.org/10.1021/ ja105482k
- Takachi, M., Matsuda, T., Moritomo, Y.: Cobalt hexacyanoferrate as cathode material for Na⁺ secondary battery. Appl. Phys. Express 6, 025802 (2013). https://doi.org/10.7567/ apex.6.025802
- 110. Zhang, Q., Wang, Z.J., Zhang, S.L., et al.: Cathode materials for potassium-ion batteries: current status and perspective. Electrochem. Energy Rev. 1, 625–658 (2018). https://doi.org/10.1007/s41918-018-0023-y
- 111. Chen, L., Gu, Q.W., Zhou, X.F., et al.: New-concept batteries based on aqueous Li⁺/Na⁺ mixed-ion electrolytes. Sci. Rep. 3, 1–7 (2013). https://doi.org/10.1038/srep01946
- Dahn, J.R., Seel, J.A.: Energy and capacity projections for practical dual-graphite cells. J. Electrochem. Soc. 147, 899 (2000). https://doi.org/10.1149/1.1393289
- 113. Wu, X.Y., Qi, Y.T., Hong, J.J., et al.: Rocking-chair ammonium-ion battery: a highly reversible aqueous energy storage system. Angew. Chem. 129, 13206–13210 (2017). https://doi.org/10.1002/ange.201707473
- Li, C., Wu, J., Ma, F., et al.: High-rate and high-voltage aqueous rechargeable zinc ammonium hybrid battery from selective cation intercalation cathode. ACS Appl. Energy Mater. 2, 6984–6989 (2019)
- Knight, C., Voth, G.A.: The curious case of the hydrated proton. Acc. Chem. Res. 45, 101–109 (2012). https://doi. org/10.1021/ar200140h
- Yan, L., Huang, J.H., Guo, Z.W., et al.: Solid-state proton battery operated at ultralow temperature. ACS Energy Lett. 5, 685–691 (2020). https://doi.org/10.1021/acsenergylett.0c001 09
- Crumbliss, A.L., Lugg, P.S., Morosoff, N.: Alkali metal cation effects in a Prussian blue surface modified electrode. Inorg. Chem. 23, 4701–4708 (1984). https://doi.org/10.1021/ic001 94a057
- 118. Lee, H.W., Pasta, M., Wang, R.Y., et al.: Effect of the alkali insertion ion on the electrochemical properties of nickel hexacy-anoferrate electrodes. Faraday Discuss. 176, 69–81 (2014). https://doi.org/10.1039/c4fd00147h
- Feiner, A.S., McEvoy, A.J.: The Nernst equation. J. Chem. Educ.
 493 (1994). https://doi.org/10.1021/ed071p493
- Wang, X.F., Bommier, C., Jian, Z.L., et al.: Hydronium-ion batteries with perylenetetracarboxylic dianhydride crystals as an electrode. Angew. Chem. 129, 2955–2959 (2017). https://doi.org/10.1002/ange.201700148

- Agmon, N.: The Grotthuss mechanism. Chem. Phys. Lett. 244, 456–462 (1995). https://doi.org/10.1016/0009-2614(95)00905-j
- 122. Cukierman, S.: Et tu, Grotthuss! And other unfinished stories. Biochim. Biophys. Acta 1757, 876–885 (2006). https://doi.org/10.1016/j.bbabio.2005.12.001
- 123. Wu, X.Y., Hong, J.J., Shin, W., et al.: Diffusion-free Grotthuss topochemistry for high-rate and long-life proton batteries. Nat. Energy 4, 123–130 (2019). https://doi.org/10.1038/s4156 0-018-0309-7
- 124. Wu, X.Y., Qiu, S., Xu, Y.K., et al.: Hydrous nickel–iron Turnbull's blue as a high-rate and low-temperature proton electrode. ACS Appl. Mater. Inter. 12, 9201–9208 (2020). https://doi.org/10.1021/acsami.9b20320
- 125. Jiang, H., Shin, W., Ma, L., et al.: A high-rate aqueous proton battery delivering power below -78 °C via an unfrozen phosphoric acid. Adv. Energy Mater. **10**, 2000968 (2020). https://doi.org/10.1002/aenm.202000968
- Liang, G.J., Mo, F.N., Yang, Q., et al.: Commencing an acidic battery based on a copper anode with ultrafast proton-regulated kinetics and superior dendrite-free property. Adv. Mater. 31, 1905873 (2019). https://doi.org/10.1002/adma.201905873
- 127. Wang, Y., Zhong, H., Hu, L., et al.: Manganese hexacyanofer-rate/MnO₂ composite nanostructures as a cathode material for supercapacitors. J. Mater. Chem. A 1, 2621–2630 (2013). https://doi.org/10.1039/c2ta01354a
- 128. Wu, X.Y., Xu, Y.K., Zhang, C., et al.: Reverse dual-ion battery via a ZnCl₂ water-in-salt electrolyte. J. Am. Chem. Soc. **141**, 6338–6344 (2019). https://doi.org/10.1021/jacs.9b00617
- 129. Lee, E., Kim, D.H., Hwang, J., et al.: Soft X-ray absorption spectroscopy study of Prussian blue analogue ACo[Fe(CN)₆]H₂O nano-particles (A = Na, K). J. Korean Phys. Soc. **62**, 1910–1913 (2013). https://doi.org/10.3938/jkps.62.1910
- Kamioka, H., Nakada, F., Igarashi, K., et al.: Transient photo-induced phenomena in vacancy-controlled Co-Fe cyanides. J. Phys. Conf. Ser. 148, 012031 (2009). https://doi. org/10.1088/1742-6596/148/1/012031
- 131. Igarashi, K., Nakada, F., Moritomo, Y.: Electronic structure of hole-doped Co-Fe cyanides: Na_{1.60-δ}Co[Fe(CN)₆]_{0.90}·2.9H₂O(0.0 ≤ δ ≤ 0.85). Phys. Rev. B 78, 235106 (2008). https://doi.org/10.1103/physrevb.78.235106
- 132. Bácskai, J., Martinusz, K., Czirók, E., et al.: Polynuclear nickel hexacyanoferrates: monitoring of film growth and hydrated counter-cation flux/storage during redox reactions. J. Electroanal. Chem. 385, 241–248 (1995). https://doi.org/10.1016/0022-0728(94)03788-5
- 133. García-Jareño, J.J., Giménez-Romero, D., Vicente, F., et al.: EIS and AC-electrogravimetry study of Pb films in KCl, NaCl, and CsCl aqueous solutions. J. Phys. Chem. B 107, 11321–11330 (2003). https://doi.org/10.1021/jp035387h
- 134. Agrisuelas, J., García-Jareño, J.J., Vicente, F.: Identification of processes associated with different iron sites in the Prussian blue structure by in situ electrochemical, gravimetric, and spectroscopic techniques in the DC and AC regimes. J. Phys. Chem. C 116, 1935–1947 (2012). https://doi.org/10.1021/jp207269c
- Ventosa, E., Paulitsch, B., Marzak, P., et al.: The mechanism of the interfacial charge and mass transfer during intercalation of alkali metal cations. Adv. Sci. 3, 1600211 (2016). https://doi. org/10.1002/advs.201600211
- Yun, J., Pfisterer, J., Bandarenka, A.S.: How simple are the models of Na intercalation in aqueous media? Energy Environ. Sci. 9, 955–961 (2016). https://doi.org/10.1039/c5ee03197d



- Niu, C.J., Lee, H., Chen, S.R., et al.: High-energy lithium metal pouch cells with limited anode swelling and long stable cycles. Nat. Energy 4, 551–559 (2019). https://doi.org/10.1038/s4156 0-019-0390-6
- 138. Wan, P., Xie, H., Zhang, N., et al.: Stepwise hollow Prussian blue nanoframes/carbon nanotubes composite film as ultrahigh rate sodium ion cathode. Adv. Funct. Mater. 30, 2002624 (2020). https://doi.org/10.1002/adfm.202002624
- Yuan, X.H., Ma, F.X., Zuo, L.Q., et al.: Latest advances in high-voltage and high-energy-density aqueous rechargeable batteries. Electrochem. Energy Rev. (2020). https://doi.org/10.1007/s4191 8-020-00075-2
- Shin, J., Choi, J.W.: Opportunities and reality of aqueous rechargeable batteries. Adv. Energy Mater. 10, 2001386 (2020). https://doi.org/10.1002/aenm.202001386
- Luo, J.Y., Cui, W.J., He, P., et al.: Raising the cycling stability of aqueous lithium-ion batteries by eliminating oxygen in the electrolyte. Nat. Chem. 2, 760–765 (2010). https://doi.org/10.1038/ nchem.763
- Borodin, O., Self, J., Persson, K.A., et al.: Uncharted waters: super-concentrated electrolytes. Joule 4, 69–100 (2020). https://doi.org/10.1016/j.joule.2019.12.007



Shen Qiu received her Ph.D. degree (2016) in the Chemistry Department from Wuhan University, China. Presently, she has been working as a visiting scholar at Oregon State University. Her research direction is the development of new electrode materials for both non-aqueous and aqueous Na-ion batteries.



Yunkai Xu received his bachelor degree from China University of Petroleum in 2017. Currently, he is a Ph.D. student in Prof. Xiulei Ji's group at Oregon State University. His research direction focuses on the design of novel battery systems such as protonion batteries and dual-ion batteries.



Xianyong Wu obtained his B.Sc. (2011), M.Sc. (2013), and Ph.D. (2016) degrees in the Chemistry Department from Wuhan University, China. From 2016 to 2019, he has been working as a postdoctoral researcher in Prof. Xiulei Ji's group at Oregon State University. Currently, he works as a postdoctoral researcher at the University of Washington. His research interest focuses on the development of novel rechargeable batteries, such as proton, ammonium, and anionbased batteries.



Xiulei Ji graduated from Jilin University with a B.Sc. in chemistry in 2003. He obtained his Ph.D. degree from the University of Waterloo in 2009. He was an NSERC Postdoctoral Fellow at the University of California, Santa Barbara from 2010 to 2012. Dr. Ji is currently an Associate Professor at the Department of Chemistry, Oregon State University. His research interests are design principles of electrochemical energy storage, and materials chemistry in batteries and pseudocapacitors.

